THESIS FOR THE DEGREE OF DOCTOR OF PHILOSOPHY

ALL-OPTICAL CONTROL OF MOLECULAR FUNCTIONS – ENERGY TRANSFER SWITCHING AND INFORMATION PROCESSING

MAGNUS Å. BÄLTER

Department of Chemistry and Chemical Engineering
CHALMERS UNIVERSITY OF TECHNOLOGY
Gothenburg, Sweden 2016

All-Optical Control of Molecular Functions – Energy Transfer Switching and Information Processing
Magnus Å. Bälter
ISBN: 978-91-7597-398-2

Doktorsavhandlingar vid Chalmers tekniska högskola
Ny serie Nr 4079
ISSN: 0346-718X

Department of Chemistry and Chemical Engineering
Chalmers University of Technology
SE-412 96 Gothenburg
Sweden
Telephone: +46 (0)31 772 1000

Front cover: Photochromic emission color tuning in polymer micelles.

Back cover: Photo of the author. © Magnus Å. Bälter, 2016

Printed by Chalmers Reproservice
Gothenburg, Sweden, 2016

ALL-OPTICAL CONTROL OF MOLECULAR FUNCTIONS – ENERGY TRANSFER SWITCHING AND INFORMATION PROCESSING

MAGNUS Å. BÄLTER

Department of Chemistry and Chemical Engineering
Chalmers University of Technology

ABSTRACT

In this work, the photoswitching of molecular systems endowed with photochromic functionality have been investigated for the reversible photonic gating of excitation energy transfer (FRET) reactions as well as in application for all-photonic molecular logic. The presented systems involves the integration of photochromic entities within both covalent and non-covalent designs and serves to implicate photonic switching of molecular level phenomena. In particular, all systems include the photochromic modulation of fluorescence emission in response to photonic stimuli.

In the first part of this thesis, paper I and II, two different molecular logic systems were designed as to investigate the possibility of using photochromic molecular functions with fluorescent read-out as new possible logic platforms in all-photonic information processing and data storage. In paper I, we present the utilization of a fluorescent photochromic fulgimide derivative in combination with non-linear (SHG/THG) crystals and Nd:YAG lasers for the successful implication of an all-photonic molecular D-flip flop. In paper II, we show the covalent integration of photochromic fulgimide and dithienylethene derivatives into two different photochromic triads, resulting in a "neuron"-like *off-on-off* fluorescence emission behavior in response to illumination with UV-light, which allowed the implication of an all-photonic molecular parity generator/checker.

In the second part, papers III and VI, the possibilty for using photochromic compounds in the construction of photoresponsive supramolecular assemblies was explored. In paper III, we show the reversible photoswitching of excitation energy transfer between a donor-acceptor (FRET) pair appended to a DNA-template by photochromic modulation of the DNA-binding properties of an amidine-substituted spiropyran derivative. In paper IV, we show dichromatic emission color-tuning and generation of virtually perfect white light fluorescence by regulation of FRET communication between a donor fluorophore and a fluorescent photoswitch encapsulated in polymer micelles.

Keywords: energy transfer, photochromism, molecular logic, all-photonic, DNA-binding, photoswitch, spiropyran, fulgimide, diarylethene, dithienylethene, white-light generation, fluorescence modulation

LIST OF PUBLICATIONS

This thesis is based on the following publications and manuscript, referred to by Roman numerals in the text.

I. "An All-Photonic Molecule-Based D Flip-Flop"
Patricia Remón, Magnus Bälter, Shiming Li, Joakim Andréasson, Uwe Pischel
J. Am. Chem. Soc, **2011**, 133, 20742-20745

II. "An All-Photonic Molecule-Based Parity Generator/Checker for Error Detection in Data Transmission"
Magnus Bälter, Shiming Li, Jesper R. Nilsson, Joakim Andréasson, Uwe Pischel
J. Am. Chem. Soc, **2013**, 135, 10230-10233.

III. "Reversible Energy-Transfer Switching on a DNA Scaffold"
Magnus Bälter, Martin Hammarson, Patricia Remón, Shiming Li, Nittaya Gale, Tom Brown, and Joakim Andréasson
J. Am. Chem. Soc, **2015**, 137, 2444-2447

IV. "Emission Color Tuning and White-Light Generation Based on Photochromic Control of Energy Transfer Reactions in Polymer Micelles"
Magnus Bälter, Shiming Li, Masakazu Morimoto, Sicheng Tang, Jordi Hernando, Gonzalo Guirado, Masahiro Irie, Françisco M. Raymo, and Joakim Andréasson
Complete manuscript, submitted to Chemical Science

CONTRIBUTION REPORT

I. The author's contribution to the publication was the characterization of the fulgimide photochromic behavior. Performed a parallel study on an alternative photochromic dyad system which was not included because of lesser performance than the presented fulgimide.

II. The author performed all the spectroscopic experiments. Took part in the experimental evaluation.

III. The author performed all the spectroscopic experiments, optimized the system's performance and evaluated the experimental results. Took part in the design of the system.

IV. The author performed all the spectroscopic experiments, optimized the system's performance and evaluated the experimental results. Took part in the design of the system. Drafted the manuscript.

Table of Contents

1. Introduction

Photochromic molecules are compounds which upon absorption of light may undergo rearrangement of chemical bonds with resulting interconversion between two distinct isomeric forms. These structural rearrangements give rise to variations in absorption spectra and consequently the two isomers exhibit different colors. It is the associated color change of the photoinduced transformation that has given the chemical phenomenon of photochromism its name. As given from the Greek words "*phos* – light" and "*chroma* – color", the name photochromism thus implies light-induced change in color. Commonly, one of the forms is colorless – within absorption maximum residing in the UV-range – and the second form is colored, as it also absorbs in the visible range.

The photoinduced interconversion between the photochromic isomers does not only alter the absorption spectrum and color but does also, to varying degree, affect a number of chemical and physical properties e.g. fluorescence quantum yield, degree of conjugation, polarity, conductivity, and oxidation/reduction potentials.[1-5] Thus, the strength and versatility of photochromic compounds are derived from their inherent bistability and the distinct characteristics of their two different isomers. As such, they provide a functional motif that can be incorporated within molecular and/or supramolecular systems in order to enable remote spatiotemporal gating of molecular properties via photonic stimuli.[6-12] In fact, the photochromic phenomenon has been successfully implemented in such diverse fields as molecular logic and information storage[10-30], photoswitching of host-guest interactions and ion-affinity,[31-34] functional probes for cell-imaging,[35, 36] photo-controlled enzyme-activity,[37] DNA hybridization,[38] organic field-effect transistor[39], conductance modulation of single-molecule junctions[40, 41], induced hyper-polarizability[42], and energy and/or electron transfer modulation.[6-9, 43-60]

In most applications, it is preferable to have an easily accessible read-out of the photochromic state. Therefore, photochromic molecules that exhibit distinct emissive properties of the two photochromic forms are both highly interesting and desirable. Inherent changes in fluorescence emission associated with the photoinduced interconversion can be found for many photochromic families such as diarylethenes,[61] spiropyrans,[62] fulgimides,[63] dihydroazulenes,[64] and dihydroindolizines.[65] Typically, the fluorescence quantum yield of these compounds are very low ($\phi_F < 0.05$).

An alternative approach for achieving photoswitchable fluorescence is the covalent integration of a photochromic motif with a suitable fluorophore, resulting in the formation of a molecular *dyad*.[6-9] Commonly, the fluorescence response of these dyadic systems are modulated *via* photoswitching of intramolecular energy and/or electron transfer reactions. This strategy allows for higher degree of tunability of the desired emissive properties as well as the fact that most commercially available fluorophores exhibit much higher fluorescence quantum yields than the inherently fluorescent photochromic molecules. In fluorescence modulation based on energy transfer reactions, the change in absorption associated with the photochromic isomerization is utilized to control the spectral overlap between the emission of a donor fluorophore and the

absorption of the photochromic acceptor. Hence, by photonically activating/deactivating the intramolecular energy transfer reaction, the quenching of the excited state donor and the resulting fluorescence emission intensity can be regulated. Similarly, in systems based on electron transfer, the changes in redox potentials related to the interconversion of the photochromic moiety are harnessed to regulate the driving force of photoinduced electron transfer (PET) quenching. Thus, photonic switching of the fluorescence emission output is enabled.

These same design principles for photochromic fluorescence modulation can be incorporated within photoactive supramolecular assemblies. One such supramolecular strategy, which enables the self-assembly of supramolecular photonic nano-devices, is illustrated by the field of DNA photonics.[66] Here, DNA templates are used as scaffolds for the spatial organization of photoactive building blocks by employing the inherent Watson-Crick base-paring mechanism and the self-assembly properties of DNA hybridization. Thus, it is possible to create nanosized DNA-architectures and provide base-specific functionalization with sub-nanometer precision. Early examples are photonic wires[67-70], where multiple fluorophores are positioned on a DNA-duplex to generate a FRET cascade, which enables directional transfer of photonic energy along the DNA-axis. More complex systems include for example a photonic waveguide[71] and DNA-based artificial light-harvesting antennae.[72, 73]

An alternative supramolecular strategy involves the encapsulation of photoactive guest molecules within the self-assembled micelles formed by amphiphilic polymers.[8, 74, 75] As such, the entrapped guest are located in close proximity and can be designed to interact upon photoexcitation and exchange electrons and/or energy. Due to the self-assembly nature of these systems, the active components can be easily varied and does not require synthetic effort in the same extent as the covalent integration of photoactive compounds do.

In summary, the work presented in this thesis involves the incorporation of photochromic functionalities within molecular logic gates and photonic devices with photoresponsive fluorescence output. The first two papers (I and II) involved the realization of photochromic molecular logic gates and all-photonic information processing. Here, the photochromic interconversions and the associated variations in fluorescence emission intensities are represented as binary states (1 and 0). By subjecting the systems to various sets of photonic input signals, each input combination will give rise to a different photonic output signal. Thus, the overall photochemical response pattern to photonic stimuli allows for the interpretation of simple logic operations and processing of information. In the third paper, the photochromic phenomenon is used to implicate reversible switching of intermolecular energy transfer of a donor-acceptor (FRET) pair situated on a DNA-template. By taking advantage of the simultaneous isomerization induced alteration of the DNA-binding affinity and spectral changes of a photochromic spiropyran, the DNA intercalation of the planar merocyanine form and concomitant interception of the donor-acceptor FRET communication can be gated photonically. Finally, in paper IV, tuning of the fluorescence emission color of a multicomponent FRET system, encapsulated in polymer micelles, is achieved by photochromic modulation of intermolecular energy transfer reactions.

2. Fundamentals

2.1 Light and matter

The precise nature of light is a question that has puzzled philosophers and scientist alike throughout history. The central question has been – what is the correct description of light? Should it be described as a particle or a wave? In fact, both of them are simultaneously right. With our current understanding, a complete description of the nature of light is given by the *wave-particle duality*. This means that sometimes light behaves like a wave and sometimes like a particle. In terms of the wave aspect, classical physics and the Maxwell equations offer us the description of light as electromagnetic radiation – an oscillating electromagnetic field with orthogonal electric and magnetic components – spreading as a harmonic wave as it propagates through space. On the other hand, the particle aspect is given by quantum mechanics and proposes that light consists of photons - quantized energy packets and massless elementary particles.

The energy of a photon is given by the Planck equation:

$$E = hv$$

which states that the energy of a photon is proportional to the frequency of oscillation v of the electromagnetic field and the proportionality constant h which is referred to as Planck's constant. The frequency v is given as:

$$v = \frac{c}{\lambda}$$

where c is the speed of light and λ the wavelength of the electromagnetic radiation. In the interaction of light with matter, which exist in discrete energetic states, the energy of the light must match the difference in energy of the final and initial state. This is known as Bohr's frequency condition.

$$\Delta \mathrm{E} = \mathrm{E}_{final} - E_{initial} = hv$$

In photoexcitation, that is, the absorption of an incident photon by a molecule, the molecule undergoes an electronic transition. The absorbed energy of the photon promotes an electron from a lower to an energetically higher orbital, and the molecule is said to be in an *electronically excited state*. Furthermore, absorption of light requires that a component of the electromagnetic radiation is aligned with the transition dipole moment of the molecule. The degree of absorption that takes places as light of a given intensity (I_0) passes through a solution of given concentration is dictated by Lambert Beers law.

$$A(\lambda) = log\frac{I_0}{I} = \varepsilon(\lambda)cl$$

where ε is the molar absorption coefficient, c the concentration of the solution and l the pathlength of the light.

2.2 Excited state dynamics

Upon absorption of light, a molecule M is excited from the ground state to an electronically excited state M^*:

$$M + hv_i \rightarrow M^*$$

In the excited state M^*, the molecule will eventually return to the electronic ground state through a combination of radiative and/or non-radiative decay processes. The fate of the molecule in the excited state is efficiently summarized and described by the Jablonski diagram (Figure 1).

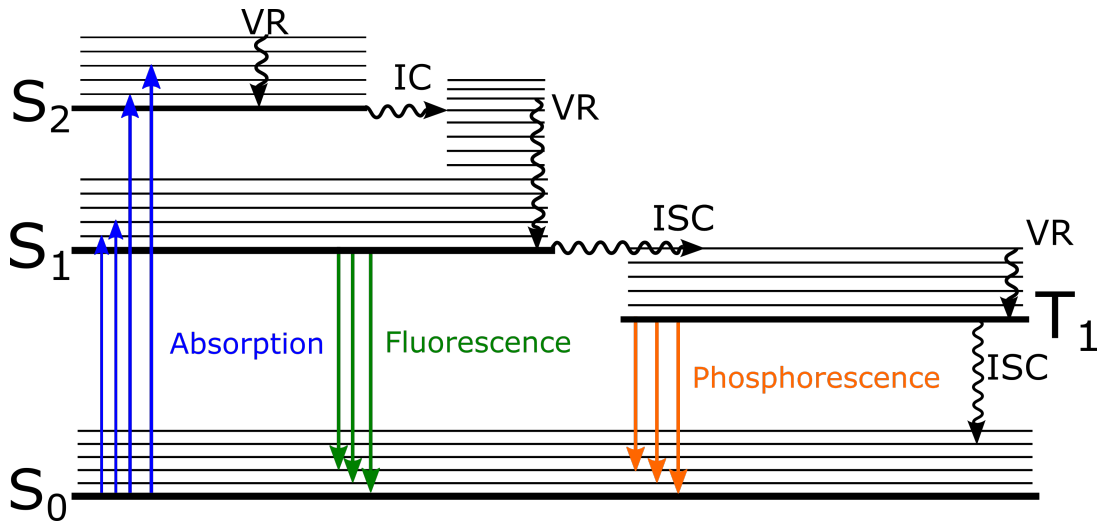

Figure 1. Jablonski diagram representing the non-radiative and radiative processes involved after the promotion of a molecule to an electronically excited state.

The pathways of non-radiative decay include vibrational relaxation (VR), internal conversion (IC) and intersystem crossing (ISC). Vibrational relaxation involves the dissipation of vibrational energy to kinetic modes of the excited molecule and solvent molecules and internal conversion the isoenergetic transition between the potential energy surface of a higher excited state (S_n) and that of a lower excited state (S_{n-1}). Intersystem crossing is the isoenergetic spin-conversion from a singlet to a triplet state.

Radiative decay is the direct transition from an electronically excited state (singlet or triplet) to the ground-state (S_0) with resulting emission of electromagnetic radiation. Fluorescence normally proceeds from an excited singlet-state (S_n) to the ground-state (S_0). As the singlet state has paired spin, the transition is quantum mechanically *allowed* and occurs rapidly (~10^8 s^{-1}). Phosphorescence refers to the transition from an excited triplet state (T_n) to the electronic ground-state (S_0). The triplet state, however, has a non-paired spin configuration and the transition is quantum mechanically *forbidden*. This means that even though the transition actually does occur, it is much slower and the excited triplet state is therefore more much long-lived than the singlet excited state. As fluorescence emission is the main radiative process in this thesis, phosphorescence will not be further discussed.

As the rate of vibrational relaxation is more rapid the rate of radiative decay, fluorescence emission takes places from a vibrationally relaxed singlet excited state (S_n). Furthermore, as the rate of internal conversion between higher electronically excited states is faster than the rate of radiative decay, fluorescence emission commonly proceeds from the lowest laying singlet excited state (S_1). This is known as Kasha's rule. Consequently, as the absorption occurs at higher energy than the fluorescence emission, this gives rise to a difference in observed absorption and emission spectra (Figure 2).

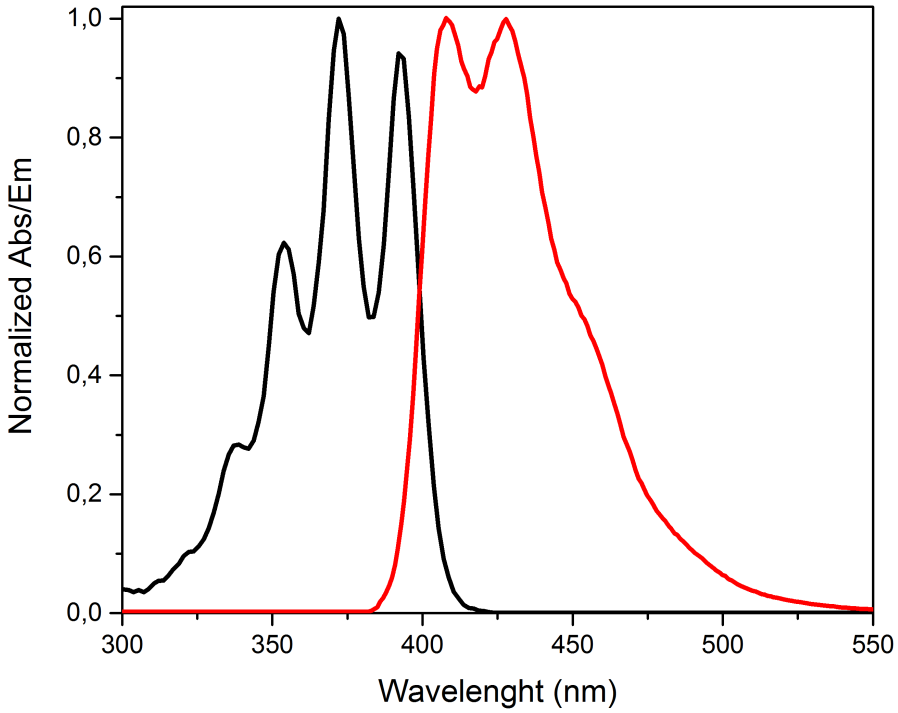

Figure 2. Normalized absorption (black) and emission (red) spectrum of 9,10-diphenylanthracene.

A further implication of Kasha's rule is Vavilov's rule, which state that the fluorescence quantum yield of a given fluorophore normally is independent of the excitation wavelength.

It is of interest to know the possibility of decay of an excited state through a specific photophysical process. The quantum yield describes the number of times a specific event occurs per absorbed photons:

$$\phi = \frac{\#\ of\ events}{\#\ of\ absorbed\ photons}$$

The fluorescence quantum yield (ϕ_f) is expressed as the rate of decay through fluorescence (k_f) over the sum of the rate of all decay events:

$$\phi_f = \frac{k_F}{k_F + k_{nr}}$$

The lifetime of an excited state is defined as:

$$\tau = \frac{1}{k_f + k_{nr}}$$

where k_f is the rate of fluorescence decay and k_{nr} the rate of decay through all non-radiative processes. Typically, the fluorescence emission intensity of an unperturbed fluorophore in the excited state exhibits a mono-exponential decay and is described by the following expression:

$$I_t = I_0 * e^{-t/\tau}$$

2.3 Energy-Transfer Reactions

In addition to the deactivation pathways of a molecule in an electronically exited state, the excitation energy may be lost through interaction with another molecule. The energy transfer reaction is a non-radiative process that takes place between a donor in the excited state (D*) and an acceptor in the ground state (A). Given the existence of a spectral overlap of the donor emission with the absorption of the acceptor as well as sufficient donor-acceptor proximity, the excitation energy can be transferred from the donor to the acceptor according to:

$$D^* + A \rightarrow D + A^*$$

The energy transfer interactions are of two kinds — Förster or Dexter transfer. The Förster mechanism, also referred to as *Förster Resonance Energy Transfer* (FRET), involves long-range dipole-dipole interaction, which couples the deactivation of the excited state donor with a simultaneous excitation of the acceptor ground state to the excited state. In contrast, the Dexter mechanism is short-range, requiring direct orbital overlap and involving actual electron/hole exchange. The work in this thesis is primarily concerned with FRET-based energy transfer reactions, even though the Dexter mechanism in some cases cannot be excluded.

In FRET, the rate of energy transfer is dependent on the donor-acceptor spectral overlap J, the fluorescence quantum yield of the donor ϕ_D, dipole moment orientation κ^2, and donor-acceptor separation *r*. The FRET interaction of a specific D-A pair can be described by the Förster radius R_0:

$$R_0{}^6 = \frac{\phi_D \kappa^2 J * 9 \ln 10}{128 \pi^5 n^4 N_A}$$

where J is the overlap integral between - $F_D(\lambda)$ - the normalized emission spectrum and - $\varepsilon_A(\lambda)$ - the molar absorption coefficient of the acceptor:

$$J = \int F_D(\lambda) * \varepsilon_A(\lambda) * \lambda^4 \, d\lambda$$

The orientation factor κ^2 describes the relative orientation of the donor and acceptor transition dipoles, and is usually assumed to be 2/3, which correlates to the average orientation of freely rotating molecules.

The efficiency of FRET energy-transfer is defined as:

$$E_T = \frac{{R_0}^6}{{R_0}^6 + r^6}$$

As seen in the equation above, the Förster radius defines the distance at which the energy transfer efficiency is 50%. Furthermore, as the distance-dependence of the energy transfer efficiency is inverse to the sixth power, the FRET interaction is extremely sensitive to changes in donor-acceptor distances. This enables the use of a donor-acceptor pair as an excellent molecular ruler with the highest spatial resolution given at distances ~R_0.

2.4 Electron transfer

Another possible deactivation pathway for the excited state is through photoinduced electron transfer (PET). It involves an electron exchange reaction between an excited state donor (D*) and a ground state acceptor (A), which results in the generation of a charge separated state:

$$D^* + A \rightarrow D^+ + A^-$$

and may also proceed *via* hole transfer:

$$D^* + A \rightarrow D^- + A^+$$

The driving force for the electron transfer reaction is described by the Rehm-Weller equation (in its simplest form):

$$\Delta G = E_{ox}(D/D^+) - E_{red}\,(A/A^-) - \Delta G_{00}$$

where $E_{ox}(D/D^+)$ is the oxidation potential of the process:

$$D \rightarrow \ D^+ + e^-$$

and $E_{red}(A/A^-)$ the reduction potential of the process:

$$A + e^- \rightarrow A^-$$

and ΔG_{00} is the energetic difference between the excited ground-state S_0 and electronically excited state S_1 of the donor.

3. Photochromism

The term *photochromism* is used to describe the ability of certain compounds to undergo light-induced reversible changes in color. The phenomenon was first reported in 1867 by Fritzsche, who observed the light-induced bleaching of an orange-colored solution of tetracene during the day, with subsequent recovery while in the dark.[5] In 1937, Hartley describes the observation of a "*reversible formation of a polymer or isomer, both forward and backward reaction being activated by light*" during photometric determinations of the solubility of azobenzene in acetone.[76] The process was first given its name in 1950s by Hirschberg, who suggested the term photochromism, derived from the Greek words *phos* (light) and *chroma* (color).[77]

3.1 Photoisomerization

A more precise definition is given by IUPAC and states the following:

"*Photochromism is a reversible transformation of a chemical species induced in one or both directions by absorption of electromagnetic radiation between two forms, A and B, having different absorption spectra*"

$$A \underset{h\nu_2 \text{ or } \Delta}{\overset{h\nu_1}{\rightleftharpoons}} B$$

While subjected to photonic stimuli, a photochromic compound undergoes structural rearrangement of chemical bonds, typically in the form of a cyclization reaction or an E/Z-isomerization, resulting in changes in geometrical and electronic configuration. Commonly, the thermodynamically stable form A is colorless and transforms into the colored form B upon irradiation with ultraviolet (UV) light. In the B form, the photochromic interconversion is reversed via application of visible light and may also in some instances be promoted thermally. The ability to interconvert thermally between the two forms is called *thermochromism*. Further, in terms of thermal reversibility, a distinction is made between photochromic molecules which display P-type photochromism – only enabling photoinduced interconversion while being thermally irreversible – and T-type photochromism – which in addition to photoinduced isomerization also enables thermal reversibility. Aside from the pronounced color changes associated with the differences in absorption spectra, the different structures of the two forms display distinct physical properties e.g. emissive properties, molecular geometry, dipole moments, redox potentials, and more.[1, 2, 4-6, 78] It is these photoinduced changes in characteristics that make photochromic molecules so interesting, as they allows for the *in situ* manipulation and control of molecular properties by photonic stimuli.

One of the primary features of photochromic molecules is of course the ability to switch. In terms of what constitutes efficient photochromic switching, the evaluation comes down to two parameters: the isomerization quantum yields (ϕ_{iso}) and the photostationary distribution (PSD). As the photochromic reaction is an excited state process, the quantum yield of

photoisomerization expresses the intrinsic efficiency of this processes in terms of the number of generated isomers in relation to the number of absorbed photons:

$$\phi_{iso} = \frac{\#\ isomers\ generated}{\#\ absorbed\ photons}$$

The photostationary distribution, on the other hand, reflects the efficiency of interconversion of an entire population of photochromic molecules to either form. Given the continuous irradiation with light of specific wavelength λ, with time, a photochemical equilibrium will be established. Assuming the quantum yields of isomerization to be wavelength-independent, the relative concentration of the two forms is thus given by the ratio of their molar absorption coefficients (ε) and isomerization quantum yields, which determines the photostationary distribution (PSD):

$$PSD(\lambda) = \frac{[A]}{[B]} = \frac{\varepsilon_B(\lambda)\phi_{B\to A}}{\varepsilon_A(\lambda)\phi_{A\to B}}$$

In terms of functional switching, it is desirable to be able to fully interconvert between the two isomeric forms. As the colored form B generally exhibits a region of exclusive red-shifted absorption, it can be addressed individually and fully switched into colorless form A. Conversely, the absorption of the colorless form A typically overlaps with the absorption of the colored form B at all wavelengths. Therefore, the B form is not always enriched to 100%, and in order to maximize the photochromic switching to the B form, illumination is directed at spectral region where the ratio $\varepsilon_A/\varepsilon_B$ is greatest, resulting in the highest possible PSD.

The photoinduced interconversion between the isomeric forms is a reversible process. However, alternative side-reactions may occur from the excited state, which result in irreversible bond-breakage and chemical degradation. This photodecomposition reduces the number of active photochromic molecules and leads to a decrease in performance over time. In short, for most applications, the ideal photochromic molecule is one that exhibits fully reversible and 100% interconversion between both isomeric forms, has high photoisomerization quantum yields, low photochemical fatigue and high thermal stability.

3.2 Photochromic families

Within the most frequently used families of photochromic compounds, two distinct classes can be defined with regard to the nature of their structural interconversion. The first class involves molecules which undergo isomerization through photocyclization reactions and include e.g. diarylethenes (DAE), spiropyrans (SP), and fulgimides (FG). The second class are characterized by the E/Z-isomerization of a double-bond as found in azobenzenes and stilbenes. The photochromic molecules used in this thesis – fulgimide (FG), diarylethene/dithienylethene (DAE/DTE) and spiropyran (SP) – all lend themselves to the first class and undergo cyclization-based photoisomerization reactions. In the following sections their individual characteristics and areas of applications will be presented.

3.2.1 Fulgimides and fulgides

The fulgides and their derivatives, fulgimides, are part of a family of photochromic compounds, which undergo both photoinduced cyclization reactions and E/Z-isomerization (Figure 3).[3, 79] The first fulgides where synthesized in the beginning of the 20th century by Stobbe, who observed the coloration of a benzene solution of diphenylfulgide upon exposure to light.[80] The nature of the photochromic reaction was not fully known and up until the 1960s it was believed that the coloration arose from an E/Z-isomerization.[81] However, as we know today, the colorization arises from the UV-induced ring-closure reaction. The fulgimides, which are the photochromic compounds of this family used in this thesis, refer to the succinimide derivatives of the corresponding fulgides.[82]

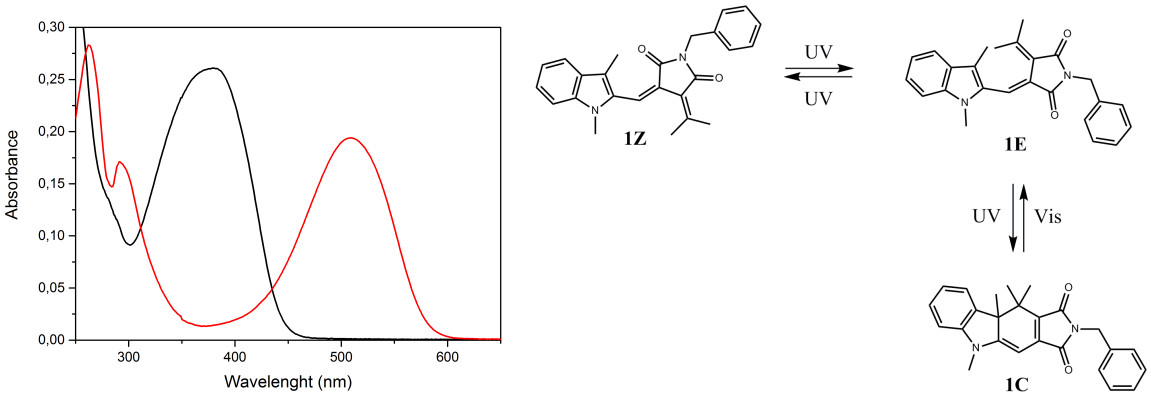

Figure 3. Left: Absorption spectra of open **1E** (black line) and closed **1C** (red line). Right: Structure and isomerization pathways of fulgimide **1** used in paper I.

The primary photochromic behavior of fulgimides is based on the 6π-electrocyclization reaction of the open-form 1, 3, 5-hexatriene motif into the 1, 3-cyclohexadiene of the ring-closed form. In addition to the cyclization reaction, the open-form also displays E↔Z interconversion and the molecule may exist in three isomers, all which are thermally stable. Due to geometrical requirements of the 6π-electrocyclization, the photoinduced ring-closure reaction can only proceed from the open E-form, as the open Z-form lacks the right conformation of the double-bonds to undergo the cyclization reaction.

In addition, UV-exposure of the open E-form do not only result in ring-closure and generation of the closed-form C but also promotes the competitive formation of open Z-form. However, as E and Z interconverts rapidly under UV-irradiation, typically quantitative switching to the closed-form C occurs anyway. The cyclization reaction is reversed by subjecting the ring-closed C-form to visible light.

The photoswitching of fulgides/fulgimides has been investigated for a number of different applications. One of them is for optical memory storage.[3, 83, 84] The fulgides/fulgimides fulfill all the basic requirements for photochromic compounds to be useful as a memories: thermal stability for long-term information storage, high photochemical fatigue resistance to enable multiple read-write-erase cycles without performance losses, and efficient photoreactions. For

example, Matsui et al. achieved an impressive 10^5 read-erase cycles with less than 20% photodegradation.[85] Furthermore, a non-destructive readout memory with extremely fast switching rates (~10^{10} s^{-1}) has been realized by utilizing polarity changes of the cyclization reaction to modulate the fluorescence of an appended fluorophore.[86]

Some photochromic fulgimides/fulgides derivatives display inherent fluorescence of the closed-form,[3, 63, 87] and their photochromism have also been utilized in switching of intramolecular energy-transfer reactions for regulation of the emission of an appended fluorophore.[44, 56] In addition, they have also found their use in the construction of photoresponsive molecular logic gates. For example, the covalent integration of a fulgimide, a porphyrin, and a dithienylethene into a molecular triad has enabled the realization of all-photonic molecular XOR/NOR logic, as well as sequential keypad functionality, with fluorescence read-out.[17, 19]

In paper I, the photochromic switching of fulgimide **1** (Figure 3) was used to provide the memory storage functionality in the implication of an in an all-photonic molecular D-flip flop. In paper II, a photochromic fulgimide derivative was covalently integrated with a photochromic diarylethene to constitute in two photoresponsive triads, which provided an *off-on-off* fluorescence behavior in response to UV-irradiation.

3.2.2 Diarylethenes and dithienylethenes

The diarylethenes (DAE) and dithienylethenes (DTE) are another major family of photochromic compounds, and the study of their synthesis, photophysical characterization and application has received massive scientific interest in the last few decades.[1, 4, 88, 89]. They are generally known for their high thermal stability and high fatigue resistance. The first thermally irreversible diarylethenes were reported in 1988 by Masahiro Irie and were synthesized on the basis of the photochemical reactions of stilbene.[90] The thermally stable E-stilbene undergoes light-induced E/Z-isomerization to form Z-stilbene, with subsequent photonic stimuli promoting the formation of the ring-closed dihydrophenanthrene via a 6π-electrocyclization reaction (Scheme 1). Finally, dihydrophenanthrene yields phenanthrene via oxidation, which is not desirable as it eliminates the possibility for further photoswitching.

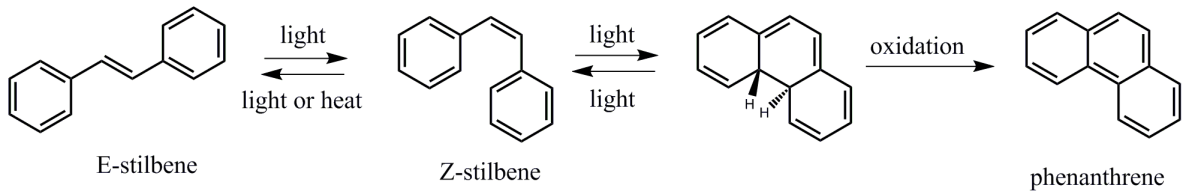

Scheme 1. Photothermal reactions of stilbene, followed by oxidation to phenanthrene

Thus, in the synthesis of diarylethenes, the hydrogen substituents of the carbons involved in the cyclization reaction are commonly replaced with methyl- or ethyl-groups in order to suppress oxidation and an aryl-bridging C=C-bond is incorporated into a cycloalkene structure to prevent the *cis* → *trans* photoisomerization. In addition, substitution of the phenyl moieties with heterocyclic aryl groups, commonly thiophene, lowers the aromatic stabilization energy of the

open-form ground-state and effectively increases the thermal stability of the closed-form.[91] Introduction of the perfluorocyclopentene motif (Figure 4) increases stability and promotes a spectral shift of the closed-ring form to longer wavelengths.[92]

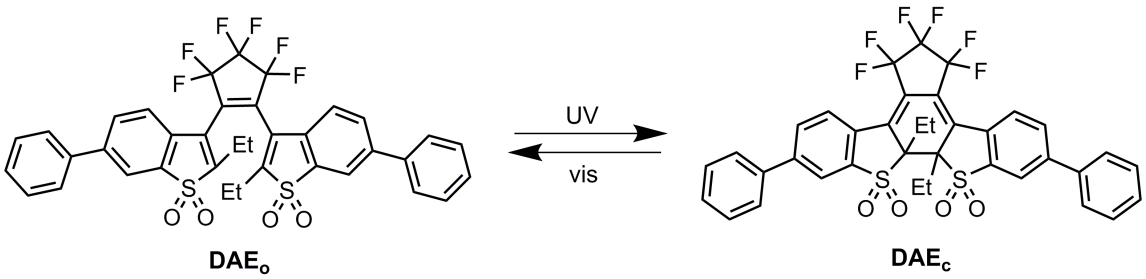

Figure 4. Structure and photoinduced interconversion of open- and closed-form diarylethene (**DAE**). UV-irradiation induces generation of the ring-closed form **DAE$_c$**. The reverse reaction is triggered by irradiation with visible light.

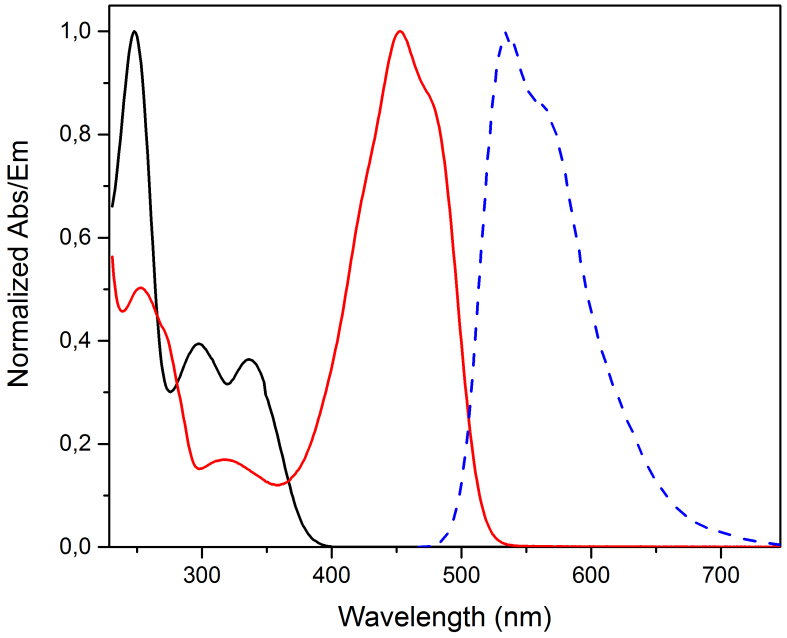

Figure 5. Absorption spectra of open-form **DAE$_o$** (solid black line) and closed-form **DAE$_c$** (solid red line), and closed-form **DAE$_c$** emission (blue dashed line).

Upon UV-induced photoisomerization the colorless open-form isomer **DAE$_o$** undergoes a 6π-electrocyclization reaction to yield the colored closed-form **DAE$_c$** isomer, with concommitant bathochromic shift in absorption due to the extended π-conjugated system (Figure 5). The photoisomerization is reversed by exposure of the closed-form to visible light, resulting in ring-opening and yielding the open-form once again. In some diarylethene derivatives, one of the photochromic isomers (typically the open form) displays exclusive fluorescence emission.[1, 61, 89, 93] However, some recently synthesized sulfone derivatives of diarylethenes presented by Uno *et al*. instead exhibit a highly fluorescent closed-form isomer.[61] In terms of molecular geometry, the changes accompanying the photochromic interconversion of diarylethenes and

dithienylethenes are small and may even allow for switching in the crystalline state.[4] However, the two forms exhibit significant difference in conformational flexibility, with the closed-form being conformationally constrained and the open-form more flexible.[94]

In solution, due to low energetic barriers, the open form interconverts thermally between a parallel and an anti-parallel conformation, and typically displays a 1:1 ratio.[4] In accordance with the Woodward-Hoffman rules[95] governing 6π-electrocyclization reactions, the photoinduced ring-closure can only proceed via the symmetry-allow conrotatory mechanism proceeding from the anti-parallel conformer of the open form. Consequently, the effective quantum yield for photocyclization in diarylethene is reduced and typically does not exceed 0.5.

The family of diarylethenes and their derivatives is diverse and the literature displays a broad-range of applications e.g. digital single-molecule fluorescence switching,[96] optical transistor,[97] memory storage with non-destructive read-out,[98] metal-complex NIR photochromism,[99] ion-recognition[100] and chemo-sensing[101, 102], two-photon 3D optical data storage[103], molecular NOR/INHIBIT gate,[25, 104] photochromic fluorescent bio-label,[105] and live-cell imaging.[106]

In paper II, a photochromic dithienylethene derivative was covalently integrated with photochromic fulgimide in the formation of two photochromic triads, which were used to implement all-photonic molecular XOR/XNOR logic for parity generation/checking. In paper IV, a fluorescent photochromic diarylethene acceptor was co-encapsulated with a donor fluorophore 9,10-diphenylanthrance in polymer micelles. Through photoswitching of the photochromic diarylethene, the intermolecular energy transfer reaction between the donor and the acceptor could be controlled photonically and resulted in tuning of the emission color.

3.2.3 Spiropyrans

The spiropyran family and their photochromic behavior was first discovered by Hirshberg in 1952.[77] The ring-closed spiro-form (**SP**) consists of two orthogonal heterocycles, an indoline and a chromene moiety, linked through the shared sp^3-hybridyzed spiro-carbon. Exposure to UV-light initiates the cleavage of the spiro-carbon C-O bond, followed by cis/trans isomerization of the C=C double-bond and finally yields the colored merocyanine form (**MC**), whose extended π-conjugated system leads to a red-shift in absorption (Figure 6).

The resulting merocyanine form is planar and zwitterionic, bearing a negatively charged phenolate oxygen and a positively charged indoline nitrogen. The phenolate oxygen can be protonated, giving the protonated merocyanine (**MCH**$^+$) with a resulting hypsochromic shift in absorption. In addition, in aqueous solution, protonation of the phenolate oxygen inhibits the thermally induced ring-closure reaction while still allowing for photoinduced isomerization back to **SP**.

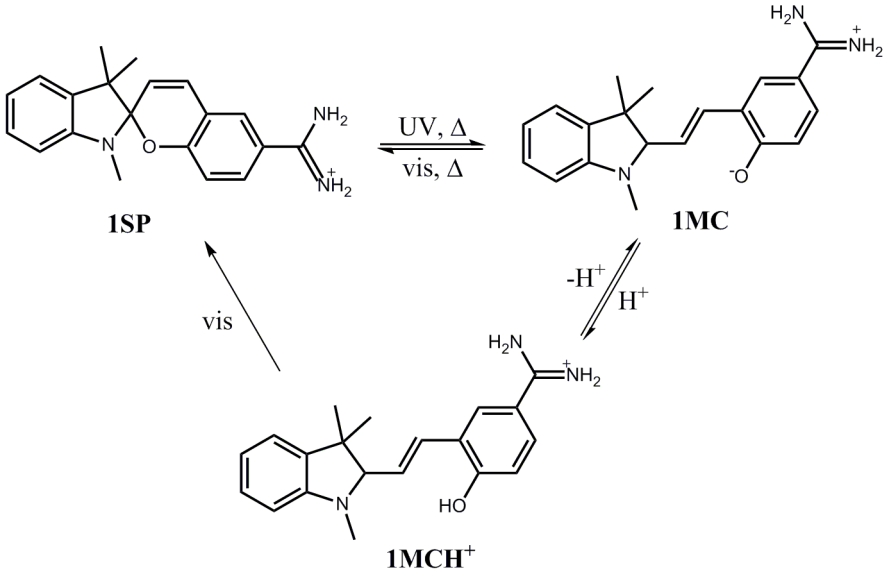

Scheme 2. Structure and schematic representation of isomerization and interconversion pathways of **SP**, **MC** and **MCH**$^+$.

Typically, in nonpolar solvents, photochromic spiropyran exist predominantly in the ring-closed spiro-form.[107] In polar solvents, however, as the zwitterionic merocyanine form becomes more energetically stabilized with increasing solvent polarity, the spiro-form undergoes a thermally induced ring-opening reaction and the thermal equilibrium is shifted towards the merocyanine form. Even though the thermal equilibrium is primarily dependent on solvent polarity, it is also effected by the nature of the spiropyran substitution patterns.[108] Similarly, the rate of thermal ring-closure of **MC** to **SP** is also solvent- and substituent dependent, ranging from a few seconds to a few hours for the establishment of thermal equilibrum.[109]. In terms of the polarity change associated with the isomeric interconversion, the resulting formation of the zwitterionic merocyanine form gives rise to a significant change in dipole moment (**MC** ~14-18 D and the **SP** ~4-6 D).[110]

In terms of geometrical changes, the spiropyran is the photochromic compound included in this thesis that exhibits the most significant structural difference between the two isomers. In fact, the pronounced geometrical transformations involved in the isomerization between **SP** and **MC** make the photochromic spiropyrans excellent compounds for photonic switching of DNA-binding affinity.[27, 111] The **SP** form is bulky and nonplanar, due to the two orthogonally oriented heterocycles, and does not bind to DNA. However, the colored MC form is planar, aromatic, and polycyclic – all characteristics known to facilitate intercalative binding interaction to DNA. Furthermore, upon protonation of the phenolate oxygen, electrostatic attraction to the negatively charged phosphate backbone increases and results in higher binding affinity.

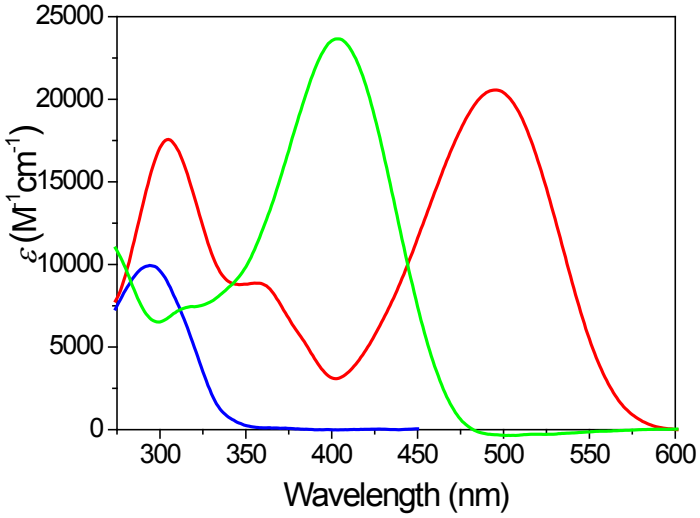

Figure 6. Absorption spectra of **SP** (blue line), **MC** (red line), and **MCH**$^+$ (green line).

Spiropyran are found in multiple areas of application.[2, 110, 112, 113] Among these are e.g. molecular logic,[10-12, 27] dielectric switching in OFETs,[114] light-induced cytotoxicity,[115] photo-controlled dynamic materials,[110] fluorescence modulation,[9, 36, 50, 116, 117], molecular memories,[2] photoswitchable ion-recognition,[31, 33, 118] and the alteration of linear and non-linear optical properties.[119]

In paper III, the amidine-substituted spiropyran (Scheme 2) was used to reversibly control the flow of excitation energy of a FRET donor-acceptor pair on a DNA template. The gating action is two-folded, utilizing both the spatial localization of the merocyanine form in the DNA template by harnessing the changes in binding affinity as well as the associated red-shift in absorption upon isomerization from the spiro-form.

4. Fluorescence modulation

As mentioned in the previous chapter, the emissive behavior of some photochromic compounds are altered in the photoinduced interconversion from one isomeric form to the other. These compounds, which typically exhibit one exclusively fluorescent isomer, offer the possibility to tune fluorescence emission intensity and/or wavelength by controlling the distribution of the photochromic isomers through photonic stimuli. Inherent fluorescent switching is displayed by a number of different photochromic families e.g. fulgimides,[63] diarylethenes,[1, 4, 61] spiropyrans,[36, 62] and dihydroazulenes.[64] However, these compounds commonly exhibit fluorescence quantum yields which are significantly lower than those of commercially available organic fluorophores. One exception is found in a new generation of highly fluorescent diarylethene derivatives developed by Irie and co-workers, which provide thermally stable photoswitching, excellent fatigue resistance and fluorescence quantum yields as high as 0.88 in 1,4-dioxane.[61]

An alternative approach to achieving photo-controlled tuning of fluorescence emission is the integration of a photochromic switch and a fluorophore into a common molecular skeleton[6, 7, 9, 52, 55, 57, 59, 60, 120-124] or supramolecular assemblies.[6-9, 36, 50, 58] By placing the photochromic switch in close proximity of the fluorophore the distinct changes in physical properties, arising from the photochromic interconversion, can be harnessed to photonically control the emission behavior of the fluorophore. More specifically, design strategies commonly utilize changes in absorption,[24, 53, 54, 57, 59, 60, 121, 122] redox potential,[13, 47, 49, 125] conjugation,[120] dipole-moment,[86] and molecular geometry.[43, 48, 126-128]

The system resulting from a covalent integration of a photochrome, a spacer/bridge and a fluorophore is commonly termed a *dyad*. These photochrome-fluorophore dyads can be made to switch fluorescence *on*/*off* by photonically stimulated interconversion between active/inactive quenching states of the photochromic modulator (Figure 7).[6, 7, 9, 52, 55, 57, 59, 60, 120-124] With the photochromic quencher in the inactive state, Q_{off}, the fluorescence emission proceeds unimpeded. However, as the photochromic component is switched into the active state, Q_{on}, the fluorophore excited state is deactivated by interaction with the photochromic unit and the excitation energy dissipates non-radiatively. Typically, the quenching process and the photochromic regulation relies upon the gating of excited-state processes such as electron and/or energy transfer reactions.[13, 24, 43, 47-49, 53, 54, 57, 59, 60, 89, 121, 122, 125-128]

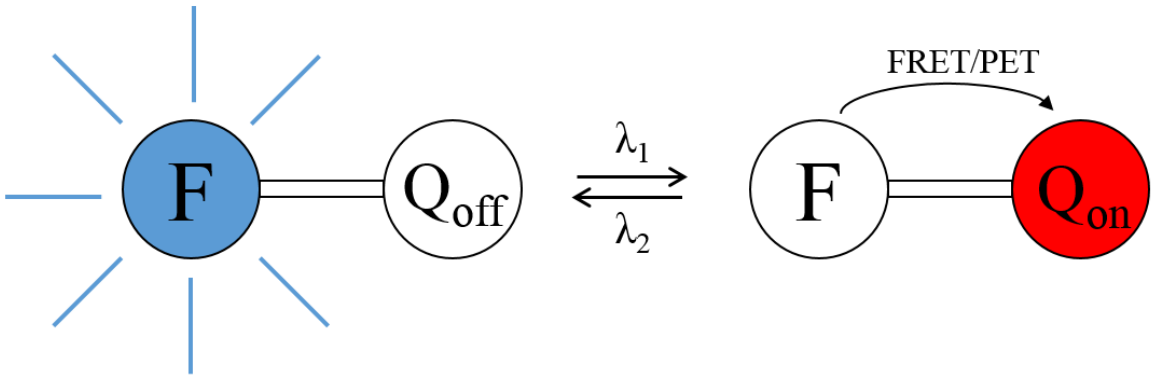

Figure 7. Schematic representation of a photochrome-fluorophore dyad. Initially, the blue fluorophore F is emitting and is unaffected by the photochromic quencher which is the inactive Q_{off} state. Irradiation with light (λ_1) induces the photochromic interconversion to the active state Q_{on} which subsequently quenches the fluorophore emission. Exposure to light (λ_2) promotes the reverse photoreaction to yield Q_{off}, alleviating the quenching and restoring the original fluorophore emission.

4.1 Electron-transfer modulation

The emissive behavior of a photochrome-fluorophore dyad can be altered on the basis of switching photoinduced electron transfer (PET) processes. In these systems, the ability to regulate emission intensity derives from the changes in redox potentials associated with the photochromic rearrangement, which can be harnessed to either suppress or activate PET process.[13, 47, 49, 125] These differences in redox potentials enables the design of systems where in one photochromic state, no driving force for electron-transfer exists, and in the other state, electron transfer processes are thermodynamically favorable. Thus, in the inactive state, the fluorophore excited state will not be affected by any photochrome-fluorophore PET interactions, whereas in the other state, it will be drained through intramolecular electron transfer between the fluorophore and photochrome components with resulting decrease in fluorescence emission intensity. In essence, by regulating the contribution of PET-based quenching to the decay of the fluorophore excited state, the relative decay through fluorescence is affected, and consequently, results in alteration of the fluorescence quantum yield.

Another strategy instead uses photochromic changes in molecular geometry to gate already thermodynamically favorable electron-transfer reactions. Here, instead of changes in redox potentials, the photochromic molecule works as to shift the distance between an electron-transfer donor-acceptor pair and results in variations in the electron transfer rates. Thus, the photochromic rearrangement indirectly governs the degree of PET-based quenching by regulating the donor-acceptor separation, which in turn alters the fluorescence quantum yield.[43, 48, 126-128]

4.2 Energy-transfer Modulation

In FRET-based fluorophore-photochrome dyads, the fluorescence modulation of the donor fluorophore relies on the photoinduced and reversible shift of the absorption of the photochromic acceptor [24, 53, 54, 57, 59, 60, 89, 121, 122]. The systems are designed such that only one of the isomers displays an absorption spectrum which overlaps with the emission of the fluorophore, and the FRET communication between the photochromic acceptor and fluorescent donor hence becomes a function of the photochromic state.

Upon activation of the intramolecular FRET pathway, the excited-state of the fluorophore is deactivated through sensitization of the photochromic component and subsequent non-radiative dissipation of the excitation energy (assuming the FRET active state of the photochromic acceptor is non-fluorescent). Thus, the photoinduced interconversion between the two isomeric forms leads to reversible gating of FRET-based fluorescence quenching and produces an *on-off*/*off-on* emission behavior (Figure 8).

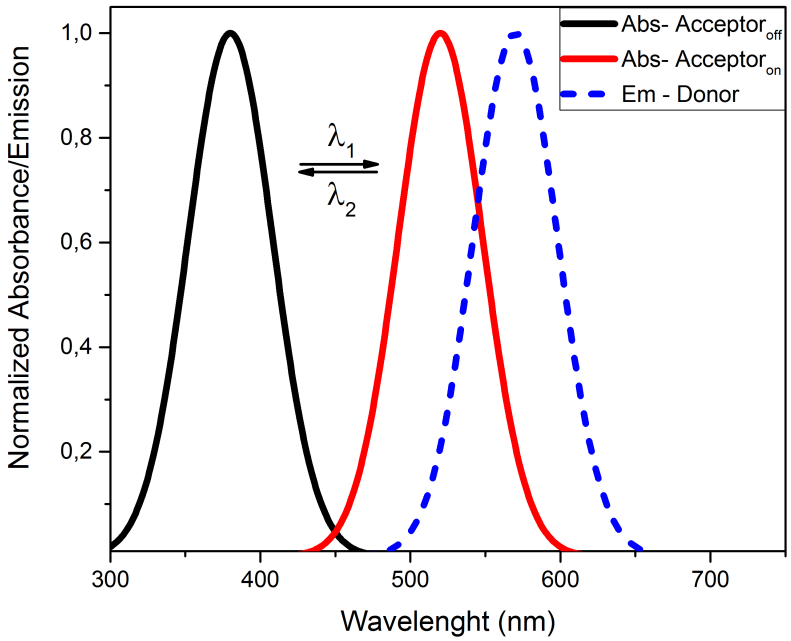

Figure 8. Theoretical absorption and emission spectra involved in the reversible switching of intramolecular energy transfer in photochrome-fluorophore dyads. Initially, as the absorption spectrum of the photochromic acceptor (black solid line) has no spectral overlap with the fluorophore emission (blue dotted line), FRET is inactive and no quenching is present. However, as exposure to light of wavelength λ_1 induces photoisomerization and switching of the photochromic state, the associated bathochromic shift in absorption (red solid line) results in spectral overlap with the fluorophore emission, activating FRET and concommitant quenching of fluorophore emission.

As a rule of thumb, photochromic molecules which exhibit large spectral shift in absorption are desirable in these designs, as this increases the individual photonic addressability of the distinct photochromic states and, hence, the possibility of enriching both isomeric forms to 100%, respectively. In addition, a large photochromic spectral shift enables higher degrees of freedom in the selection of a suitable donor fluorophore. The molar absorptivity of the photochromic acceptor and the fluorescence quantum yield of the donor should ideally be as high as possible, in order to maximize the Förster distance, R_0, of the donor-acceptor pair and thus also the energy-transfer efficiency.

In the design of FRET-based photochrome-fluorophore dyads, where the intended function is the photochromic modulation of fluorescence emission of the covalently bound fluorophore by gating of intramolecular energy-transfer processes, competitive electron-transfer reactions may pose a problem. If a driving force exists for photoinduced electron transfer involving the excited state of the photochromic component and the fluorophore ground state, this may inhibit photoswitching through competitive deactivation of excited state of the photoswitch by the PET process. Conversely, if electron transfer instead proceeds, involving the fluorophore excited state and the FRET inactive photochromic ground state, the inherent fluorescence emission may be decreased and minimize the functional window of the fluorescence switching. However, both these scenarios can be avoided by the introduction of a rigid isolating spacer which breaks π-conjugation between the fluorophore and the photochromic component to suppress or even eliminate electron transfer completely. Furthermore, if the quantum yield of photoisomerization of the energy transfer acceptor is significant, the sensitization of the photochromic excited state arising from the FRET-interaction with the fluorophore may induce undesired isomerization, which relieves the fluorophore emission quenching. In application for memory storage and molecular logic, this is termed destructive read-out.

Indeed, the abovementioned design strategies of the fluorophore-photochrome dyads may be extended to include an additional functional unit to result in the formation of photochromic triads.[117, 129-132] An example is a system with a fluorophore-photochrome-fluorophore triad consisting of a anthracene donor, a photochromic fulgide and a coumarin acceptor.[56] In the ring-open form, excitation of the anthracene donor is followed by intramolecular energy-transfer to the coumarine acceptor. However, upon UV-induced photoisomerization to the ring-closed form, energy-transfer instead proceeds to the photochromic fulgide and effectively prevents sensitization of the coumarin acceptor, resulting in a significant decrease in coumarine emission intensity. Another example, which does not exhibit fluorescence modulation but nonetheless is conceptually interesting, is given by the dithienylethene-porphyrin-fullerene triad presented by Gust et al. in 2002.[133] With the DTE in the open-form, excitation of the central porphyrin donor results in electron transfer to the fullerene acceptor and proceeds with unity quantum yield. Upon switching to the closed-form DTE, the excited state of the porphyrin is instead depopulated exclusively by intramolecular energy transfer to DTE_c.

In paper I, we show the utilization of the inherent fluorescence turn-on of a photochromic fulgimide as the effective memory storage unit in the implication of an all-photonic molecular D-flip flop.

In paper II, we present a photochromic dithienylethene-fulgimide-dithienylethene (DTE-FG-DTE) triad. Here, the fluorescence turn-on of the fulgimide is used in combination with photoinduced energy transfer quenching by closed-form DTE, resulting in an *off-on-off* fluorescence response.

In paper III, we illustrate the reversible switching of excitation energy flow between a donor-acceptor pair on a DNA template by photonically controlled DNA-binding of a photochromic spiropyran. In paper IV, the FRET switching is extended to include also a fluorescent photochromic acceptor, allowing for tuning of the emission color**.** This will be described further in the following section.

4.3 Emission color-tuning

As the fluorescence emission of organic fluorophores are not monochromatic, but rather exhibit broad emission bands, the perceived color depends on the relative distribution of photon energy and how it interacts with the cone cells of our eyes. Initially, the arbitrary nature of color perception, as it depends on each individual's ocular architecture, posed a problem in the objective comparison of different colors.

Thus, in 1931 the Commission of Internationale d'Eclairage (CIE) introduced a standardized colorimetric system – the CIE XYZ 1931 color space.[134] In this system a given spectral signature within the visible range is compared to a set function (Figure 9), a mathematically defined standard observer, which represent the chromatic response of an average human eye. The relative contribution to each color is calculated and evaluated as follows:

$$X = \int_0^\infty I(\lambda)\bar{x}(\lambda)d\lambda \qquad x = \frac{X}{X+Y+Z} \quad \text{eq. A}$$

$$Y = \int_0^\infty I(\lambda)\bar{y}(\lambda)d\lambda \qquad y = \frac{Y}{X+Y+Z} \quad \text{eq. B}$$

$$Z = \int_0^\infty I(\lambda)\bar{z}(\lambda)d\lambda \qquad z = \frac{Z}{X+Y+Z} \quad \text{eq. C}$$

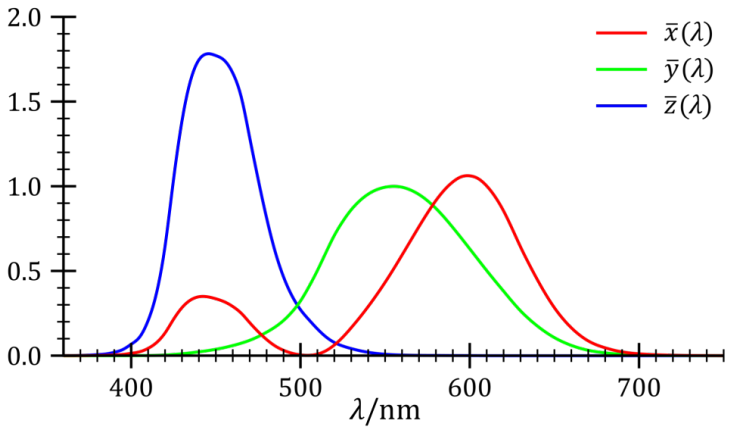

Figure 9. 1931 CIE basis functions for the normalized standard absorption of human cone receptors corresponding to the three primary colors red, green, and blue.

The spectral contribution to each of the primary colors – red (X), green (Y) and blue (Z) – is calculated as the overlap integral with the corresponding basis functions $(\bar{x}, \bar{y}, \bar{z})$ and finally yields the CIE coordinates(x, y, z). These CIE coordinates are in turned mapped in a CIE diagram and gives the perceived color of the processed spectral distribution (Figure 10).

Emission color-tuning can be obtained by additive color mixing, that is, in combining two or more distinct fluorophores in different proportions to produce a desired emission color.[135-137] In a dichromatic system, where two fluorophores are used, any color on the line joining their corresponding CIE coordinates can be achieved by controlling the relative concentration of each component. If instead a trichromatic approach is used, any color in the resulting triangular area spanned by the CIE coordinates of the three fluorophores is available. However, given the possibility of excited state energy- and/or electron-transfer processes, the resulting emission spectrum from the combination of multiple fluorophores might be quite different than the sum of their individual emission spectra. Another downside of using simple additive mixing of non-photochromic fluorophores is that the resulting color is static and requires physical access in terms of addition of material as to induce a change in the emission color.

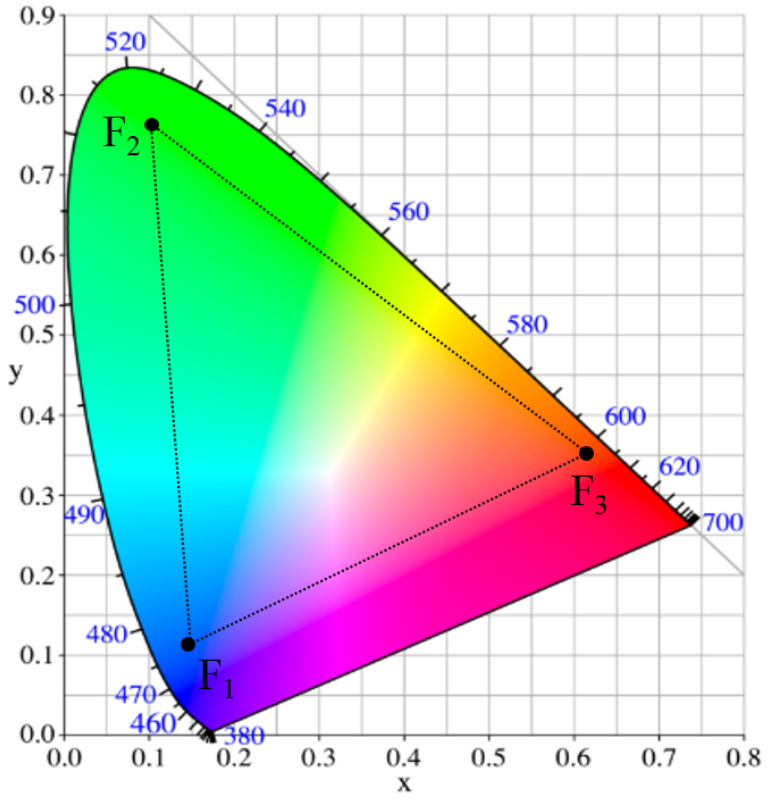

Figure 10. CIE diagram illustrating the perceived color as a function of CIE coordinates (x,y). In the dichromatic color-mixing of blue F_1 and green F_2 fluorophores, all color on the line joining their respective CIE coordinates are available through controlling their relative contribution to the overall emission spectra. In the trichromatic mixing of F_1, F_2 and F_3 all colors spanned by the resulting triangular area are available.

In fact, photochromic molecules have shown great promise in the design of FRET-based systems displaying stimuli-responsive emission color.[36, 58, 116, 124, 135, 138-140] Analogously to the photoinduced fluorescence quenching in photochromic energy transfer systems, multicolor fluorescence systems can also be constructed from fluorophore-photochrome pairs whose communication through FRET is switched on/off by shifting the absorption of the photochromic acceptors. In addition, the FRET-active form of the photochromic acceptor must in this case be fluorescent (Figure 11). With the photochromic acceptor in the inactive state, A_{off}, the acceptor is neither fluorescent nor FRET active, and only the unquenched donor fluorophore emission is observed upon excitation of the donor. However, upon switching to the active photochromic state, FRET is turned on, resulting in quenching of the fluorophore emission with concomitant sensitization and red-shifted emission of the photochromic acceptor. Assuming unity quenching efficiency, any color between the CIE coordinates corresponding to the fluorescence of the fluorescent donor and the photochromic acceptor may be achieved by the controlling the distribution of the two photochromic isomers.

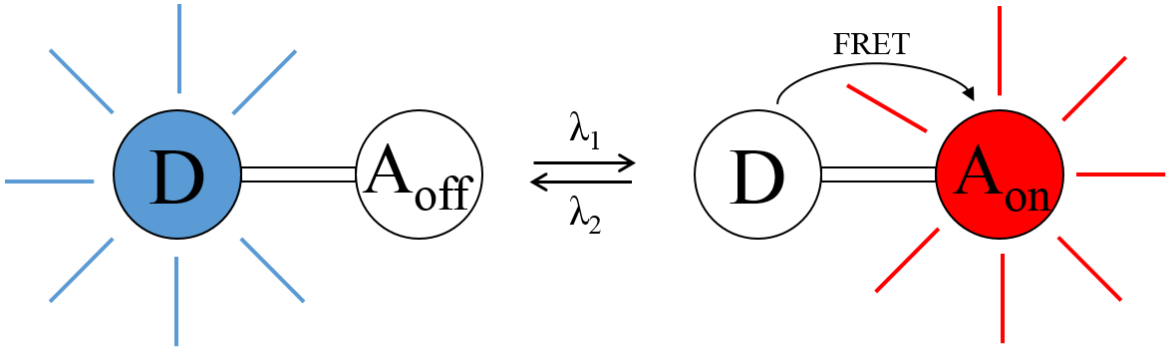

Figure 11. A donor-acceptor pair exhibiting photochromic FRET-mediated dual-color fluorescence emission. In A_{off}, intramolecular FRET is inactive, resulting in the blue donor D being the sole emitter. Exposure to light results in the formation of A_{on}, turning on the FRET and sensitizing the acceptor emission at the expense of the quenched donor emission.

An early example shows the realization of a system with reversibly photoswitchable dual-color fluorescence by combining perylene diimide with photochromic spiropyran in polymer micelles.[36] In switching from the spiro to the merocyanine form, a FRET process is activated, which quenches the fluorophore emission while simultaneously sensitizing the emission of the fluorescent merocyanine and results in a shift of emission color from green to red.

Although the research presented in the literature indeed is impressive and points the way towards new approaches in the design of future photochromic multicolor fluorescence construct, a few remaining challenges can be pinpointed. Firstly, a majority of the systems exhibit significantly lower fluorescence quantum yields of the photochromic acceptor than the fluorescent donor, leading to a compromise of overall brightness in relation to emission-color. In achieving functional systems consistent high fluorescent emission intensity, the quantum yield of the photochromic acceptor needs to be improved upon. Secondly, as the photochromic components cannot be fully interconverted between both isomers as well as less than unity

energy transfer efficiencies, this results in residual donor emission and reduces the effective magnitude of the CIE-trajectory and, hence, the extent of emission color tuning.

4.4 White-light emission

White light, as opposed to monochromatic light, consists of an energetic distribution of photons spanning a broad range of the visible spectrum of electromagnetic radiation (Figure 12). As derived from the CIE formulation, it is noted that, white-light, by definition, consists of an equal contribution to red, green and blue and is represented by the CIE coordinate (1/3, 1/3). Therefore, to satisfy the requirements of white-light emission, an emission spectrum must not only encompass a significantly broad range of wavelengths, but also exhibit a precise spectral intensity distribution with balanced contribution to each primary color.

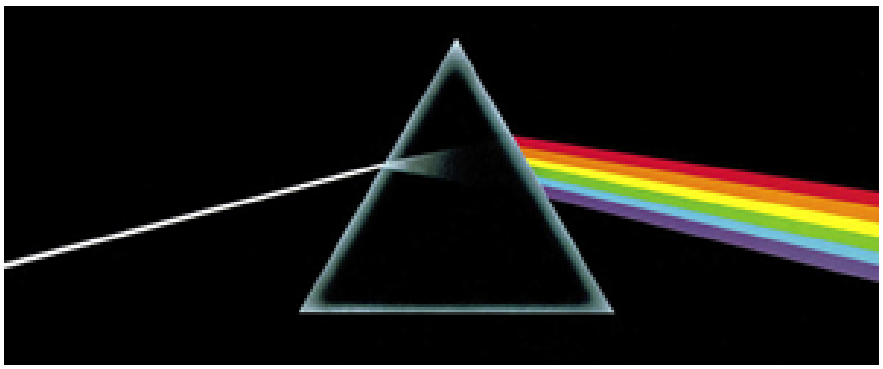

Figure 12. White light dispersed through a prism, resulting in a rainbow-like distribution of all the contained monochromatic colors (illustration from the album cover: *Dark Side of the Moon – Pink Floyd, 1973*)

Based on these conditions, it stands to reason that achieving single-molecule white-light emission is virtually impossible. In accordance with Kasha's rule, fluorophores tend to emit from the lowest laying singlet-excited state, and results in a single emission band, not nearly wide enough to satisfy the wavelength distribution condition. Similarly, integration of multiple distinct fluorophores within a common molecular skeleton, without sufficient spatial and/or electronic separation, is likely to result in intramolecular hetero-FRET and enhanced emission of the red-most fluorophore, acting as the terminal acceptor. Thus, the generation of white-light fluorescence can be regarded as a special case of emission color-tuning through additive mixing, which requires the precise combination of several distinct emissive processes to complete the simultaneous requirements of broad spectral emission and CIE coordinates (1/3, 1/3).[136, 137, 141-145] Indeed, molecular system which display, and can switch between, two distinct emission signatures has proven to be promising in the achievement of white-light. One example is given by halochromic fluorophores.[146-149] These pH-sensitive compounds exhibit various forms depending on protonation state, which vary in terms of electron delocalization and therefore may display significant changes in emission behavior. Other approaches include

formation of intramolecular exciplexes by changes in solvent polarity[150] as well as excited-state intramolecular proton transfer (ESIPT).[151, 152] However, even though a number of systems have realized multicolor emission through photochromic modulation, generation of white-light emission from such systems are rare.

In paper IV, we present the generation of virtually perfect white-light (0.32, 0.33) by reversible photochromic emission-color switching in a FRET donor-acceptor pair encapsulated in polymer micelles. Exposure to UV-light isomerizes the photochromic acceptor to the closed-form, simultaneously activating FRET communication and turning on the acceptor fluorescence. Thus, the donor emission is quenched with concomitant sensitization of the acceptor emission and results in a shift of the emission color from blue to yellow.

5. Molecular logic and information processing

The word logic is derived from the greek word "*logikos*", which can be translated into "*possessed by reason*". The act of reasoning involves the determination of the validity of an argument (true or false) in relation to a given set of parameters. This in turn can be divided into formal and informal logic. Informal logic concerns itself with arguments of a linguistic nature, such as everyday philosophical discourse ("*If a tree falls in the forest and no one is there to hear it, does it still make a sound?*") and formal logic, which relates to the more strict, symbol-bound and mathematical arguments, such as "*If A is equal to B and B is equal to C, than A must be equal to C*". The work presented in this thesis regarding molecular logic lends itself to the latter category, describing the interpretation and utilization of molecular-level chemical and photonic processes as applied to computational logic.

Computational logic involves the processing of a set of given inputs *via* a predefined logic operation to provide a set of useful outputs, thus answering the proposed argument in question. Conceptually, the operations performed within computational logic and information processing are based on Boolean algebra. In contrast to elementary algebra, which describes the application of mathematical operators to numeric variables, Boolean algebra is concerned with the operation of Boolean functions upon truth-value variables, i.e. *true* and *false*. Instead of the ordinary mathematical operators (e.g. addition and multiplication) the core Boolean functions are conjunction (AND), disjunction (OR) and negation (NOT). The truth-values, when given in a binary representation, translates into 1 (*true*) and 0 (*false*). One such binary digit is called a *bit* and is considered the basic unit of information within computational logic.

In practice, the operations of computational logic are performed by logic gates, which are physical devices that enable the implication of a given Boolean function on a set of given input values to generate the corresponding output value. For example, when using a positive logic convention in silicon-based electronic logic gates, the digital values 1 and 0 are represented as voltage high and voltage low, respectively. However, any physical property exhibiting two distinct states may be used in the representation of a bit. In addition to AND, OR and NOT gates, there are also the exclusive OR (XOR), negated OR (NOR), exclusive negated OR (XNOR) and negated AND (NAND) gates. By the integration and combination of these simple logic functions, more complex logic gates and circuitry can be created. The defined input/output response for a given logic gate or circuit is described by a *truth-table* (Figure 13).

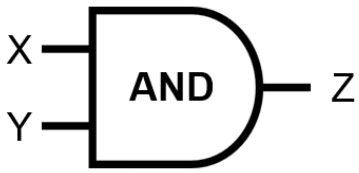

X	Y	Z
0	0	0
0	1	0
1	0	0
1	1	1

Figure 13. A schematic representation of 2-input AND logic, which combines the two inputs (X,Y) into a single output (Z) in accordance with the corresponding truth-table. As can be seen in the truth-table, the only case which results in output Z = 1 is when both inputs X = Y = 1 and the AND-argument holds *true* (1).

The first molecular logic gate was presented in the seminal work of de Silva *et al*. in 1993.[153] It involved the design and interpretation of a fluorescent molecular system capable of performing the input/output characteristics of 2-input AND logic. Furthermore, the fluorescence emission intensity could be chemically controlled by the addition of ions (Na^+ and H^+). The system consists of a fluorescent anthracene reporter conjugated to a tertiary amine and a benzocrown ether. In the absence of the cations, the amine and crown ether moieties induced significant PET-based fluorescence quenching of the anthracene fluorophore. Upon the addition of H^+ or Na^+, exclusively, slightly suppresses the PET-quenching and results in increased fluorescence by protonation of the tertiary amine (1.7-fold) or Na^+-chelation with the benzocrown ether (1.1-fold). However, the simultaneous addition of both H^+ and Na^+ results in a synergistic effect, providing an impressive 6-fold increase in fluorescence output and thus realizing AND-gate functionality.

In the last two decades, molecular logic systems have received significant attention as alternative platforms for information processing and memory storage.[1, 10-12, 20-23, 28, 154, 155] Scientific efforts has been guided by the imitation of pre-existing logic gates and circuits. Within this field, photochromic compounds stand out as promising candidates in their application in all-photonic molecular logic gates and circuits, such as AND-gate[13], half-adders[14, 125], 2:1 multiplexer/demultiplexer[15, 16], encoders-decoder[18], transistor[97] and keypad lock[19]. Firstly, due to the inherent bi-stability of the photochromic switches, the photochromic compounds provide a natural memory storage and bit-retention capability. Secondly, in contrast to molecular logic systems based on chemical inputs, which may suffer from waste accumulation in repeated cycling, the all-photonic approach is non-invasive, waste-free and enables excellent spatiotemporal control. However, a downside of molecular logic systems based on photochromic components is the possible destructive nature of the fluorescence-based read-out of state, which may disturb the state of the system and result in loss of information (see below).

In the design of all-photonic molecular logic gates, a photochromic molecule is typically integrated with a fluorophore to form a dyadic system that enables photo-controlled fluorescence modulation *via* e.g. photoinduced electron transfer (PET) or fluorescence resonance energy transfer (FRET).[6, 7, 20] In providing a photonic output signal, the evaluation

of the binary state of the switch is enabled by the measurement of the fluorescence emission intensity. In the case of memory-based applications it is essential that the implicated photochromic isomers exhibit; i) high-thermal stability to ensure reliable long-term information storage and; ii) high fatigue resistance to enable multiple write-and-erase cycles and minimize photodegeneration.

As previously mentioned, the fluorescence-based read-out of photochromic state introduces a possible caveat. As emission proceeds from the excited state and requires the excitation of the system, unless precautions are taken in the design, excitation energy may promote unwanted photoisomerization reactions and loss of information. In addition, in systems that utilize energy transfer processes as the basis of fluorescence modulation, the associated sensitization of the photochromic molecule necessary to induce the fluorescence quenching can also result in non-desired photoisomerization and distortion of state information.

The phenomenon of excitation-induced loss of data is referred to as destructive read-out and has been addressed through various strategies. Primarily, in order to create a system exhibiting distinct wavelengths for photonically addressing read, write and erase operations, the absorption of the reporter fluorophore and the photochromic switch must be spectrally separated.[86] By using photoinduced electron transfer as the mechanism for fluorescence quenching, the sensitization of the photochromic molecules by excitation energy transfer is prevented (provided that the photochromic compounds are not electrochromic) and thus inhibits any non-desired photoisomerization.[96, 156]

One of the major challenges in the field of molecular logic lies within the concatenation of single operational units into higher-order networks in the construction of complex logic systems. While electronic logic-gates use electric potential both as input and output signals as well as wires to connect the output of one gate to the input of another, molecular logic gates exhibit both an input/output inhomogeneity as well as issues with signal direction and gate-specific addressability. The input/output inhomogeneity may take the form of chemical inputs and photonic outputs. Even if the all-photonic approach is applied, the issue of intermolecular energy losses and resulting red-shift from excitation wavelength to emission wavelength remains. On the other hand, one advantage of using molecular logic gates is that they enable functional integration of complex logic functions into one single molecular structure, as opposed to electronic gates, which require the physical integration of multiple basic logic gates to achieve the same function. Furthermore, as molecular logic systems display changes in a range of physical properties (e.g. absorption, emission and redox potentials), a single molecular logic system may be able to perform a multitude of different logic operations – depending on the selection of the input and output parameters.[20]

In combinational logic systems, the output signal only depends on the current input signals, while in sequential logic systems, the output signal is dependent on both the current and previous input signals, thus enabling a memory effect. One everyday example illustrating sequential logic circuits includes the keypad lock in the ATM. This systems not only requires you to enter the right numbers of your PIN-code, but also in the right sequence. The memory effect in sequential logic circuits is achieved by the use of switches, flip-flop and latches. These

bistable memory storage elements are created by the concatenation of multiple basic logic gates with thr addition of integrated feedback loops. However, in photochromic molecular logic system, sequential logic behavior can be implemented without the need for concatenation of multiple gates and signal feedback, as thermally irreversible photochromic compounds imply an inherent memory storage functionality.

In paper I, the function, truth-table and implication of an all-photonic molecular D flip-flop is presented. In paper II, we present an all-photonic molecular XOR/XNOR logic system which enables the realization of a parity generation and checking.

6. Bio-inspired self-assembly design strategies

As mentioned before, photoresponsive molecular architectures can be constructed through number of design strategies. In this thesis, the functional integration of photochromic and fluorescent moieties (in the creation of photoswitchable energy transfer systems) involve both covalent linkage as well as supramolecular self-assembly. In the following section, as the covalent integration in terms of photochrome-fluorophore dyads/triads has already been covered in chapter 4, the background and rational of the employed supramolecular design strategies will be expanded upon.

6.1 What is DNA?

Deoxyribonucleic acid (DNA) is a biological polymer in which our genetic information is encoded. The basic building blocks of DNA are called nucleotides, and each nucleotide is in turn composed of a nucleobase, a deoxyribose sugar and a phosphate group. The nucleotides are linked together through a phosphodiester bond to form polynucleotides, or simply, single-stranded DNA. In DNA, there are four different nucleobases - adenine (A), thymine (T), guanine (C) and cytosine (C) – and only the specific pairs A-T and G-C provide each other with the corresponding hydrogen bonding motif required for Watson-Crick base-pairing. It is this selectivity of the base-paring that enables two DNA single-strands with complementary base-sequence to self-assemble, i.e. hybridize, and form a double-stranded DNA helix (Figure 14). The most common DNA double helix is the B-form, which has a right-handed helical structure with ~10 base-pairs per turn.[157] In the resulting structure, the negative phosphate backbone faces outward the aqueous environment and the hydrophobic nucleobases stack with each other as to minimize their hydrophobic interaction with the water, and the separation of two adjacent base-pairs is 3.4 Å.

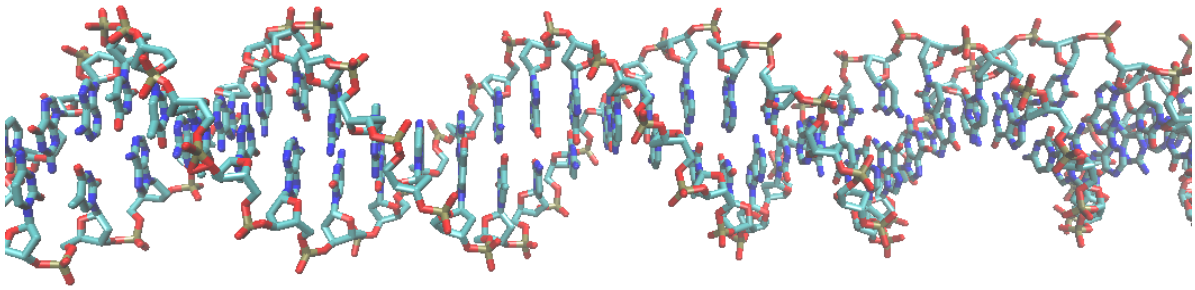

Figure 14. Illustration of the structure of the DNA double helix.

Due to the electrostatic repulsion between the negatively charged phosphate backbones, the DNA double helix requires the presence of cationic species, typically Na^+, K^+ or Mg^{2+}, to neutralize this interaction and maintain the integrity of the helical structure. Furthermore, the negative charge of the phosphate backbone enables the electrostatic attraction and association

of positively charged molecules to DNA. Binding to DNA can occur through intercalation, in which the associated molecule is inserted in between the hydrophobic bases.[158, 159] A good intercaltor is typically planar, polycyclic, hydrophobic, and positively charged e.g. ethidium bromide. In addition, interactions include binding to the major and the minor groove.

6.2 Photonic architectures on DNA scaffolds

One of the great challenges in the creation of molecular photonics lies in the controlled assembly of functional building blocks with nanometer precision, and for these purposes, DNA has proved itself to be an promising candidate.[66, 160] Primarily, the unique recognition properties of DNA base-pairing enables excellent spatial precision (sub-nm) and structural addressability for incorporation of photoactive units. The realization of photonic devices from DNA-based templates offers distinct advantages, such as automated base-sequence synthesis as well as the self-assembly nature of DNA hybridization. Furthermore, using multiple strands with different modification patterns or functionalization provides the possibility for convenient variation of e.g. acceptor-donor distances or even acceptor-donor combinations.

The first photonic "wire" based on a DNA template was reported by Uchimaru et al. in 1999.[67] The design involves a 25bp ss-DNA oligo 5'-modified with 6-carboxyfluorescein, which upon sequential hybridization of two fluorophore-modified complementary strands, establishes a three-fluorophore hetero-FRET cascade transferring excitation energy over 8 nm. This fundamental design strategy was later improved upon by Ohya et al. by the use of a mixture of hetero- and homo-FRET transfer-processes, extending the system and to achieve a 10 nm photonic wire.[68] In addition, further progress was presented by Heilemann et al. in the realization of a five-color unidirectional DNA-based photonic wire with over 90% energy-transfer efficiency extending over 13.6 nm and a spectral range of ~200 nm[69]. A more complex system is illustrated by the photonic waveguide realized by Hannestad et al.[71] It consist of three unique fluorophores – one donor and two acceptors – positioned on a self-assembled hexagonal DNA nanostructure. Initially, FRET communication proceed from the donor to the primary acceptor. Conversely, by introduction of an intercalating YO dye, a competitive homo-FRET pathway is established between the donor and the second acceptor, and consequently redirecting the flow of excitation energy. Another interesting concept is the DNA-based artificial light-harvesting antennae based on multichromophoric arrays of primary chromophores which concentrate the excitation energy to a single red-shifted emitter.[72, 73]

However impressive, the downside of the abovementioned systems lies in the irreversible nature of how donor-acceptor mediation is established. Once the intercalator dyes or ss-oligos have been introduced, there is no straightforward means to remove it without completely destroying the system. Thus, the introduction of a photoswitchable DNA binder enables the reversible operation and photonic control of the energy-transfer process, taking these photonic architectures one step further.

In paper III, a DNA template has been used as a self-assembled scaffold in the realization of an energy-transfer system. The reversible DNA-binding of a photochromic spiropyran is used to gate the energy-transfer efficiency of the DNA-appended donor-acceptor pair, resulting in a "transistor"-like behavior in response to photonic stimuli.

6.3 Micellar nanostructures

A surfactant is an amphiphilic molecule, that is, it displays both hydrophobic and hydrophilic domains. As such, in aqueous solution, surfactants tend to aggregate as the hydrophilic parts seek to maximize their interactions with the water while the hydrophobic parts seek to minimize them. The result is the self-assembly of dynamic micelles – nanostructures composed of multiple individual surfactants. However, surfactants are typically relatively small molecules, and amphiphilic character can be imposed on macromolecular structures by incorporating multiple hydrophilic and hydrophobic domains within the same polymer backbone (Figure 15).[161-166]

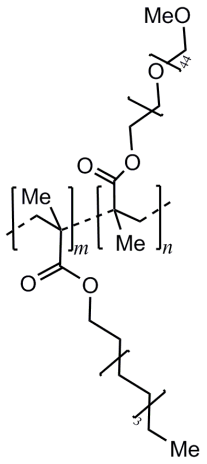

Figure 15. Structure of amphiphilic copolymer used in paper IV. It consists of a common polymer with hydrophobic decyl and hydrophilic poly-(ethylene glycol) side-chains. The ratio of hydrophobic (*m*) and hydrophobic (*n*) elements is 6:1 (*m*:*n*).

Similar to the small-molecule surfactants, the amphiphilic polymers spontaneously self-assemble into micellar nanoparticles. However, the increased interconnectivity of individual hydrophobic and hydrophilic domains results in constructs with higher structural integrity. The hydrophobic domains associate into a common hydrophobic core in order to minimize their interactions with the water, and the hydrophilic domains, on the contrary, organize on the surface of the micellar constructs, extending into the aqueous environment and enable water solubility of the overall architecture. In fact, the resulting micellar constructs function as nanosized carrier entities and enables the encapsulation of multiple photoactive hydrophobic guests within the micellar core.[8, 50, 74, 75]

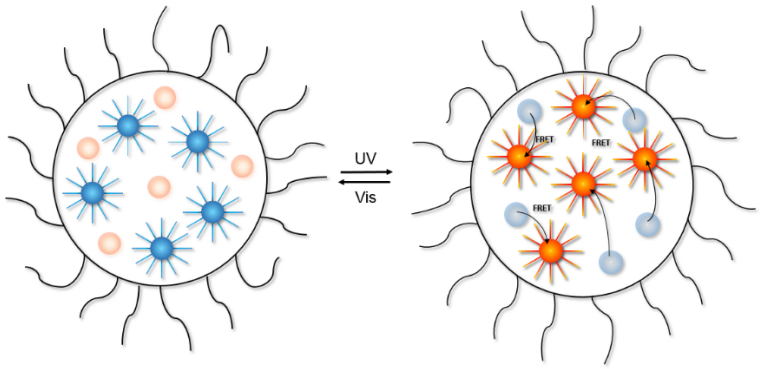

Figure 16. Schematic representation of the micellar nanoconstructs of paper IV, encapsulating a photochromic diarylethene derivative (orange) and a fluorescent 9,10-diphenylantracene (blue). Photoswitching of the photochromic diarylethene allows for photonic control of intermolecular energy transfer, resulting in emission-color tuning.

This enables the realization of multifunctional photoresponsive systems whose components interact upon light exposure to exchange e.g. energy or electrons (Figure 16). In addition to encapsulation of free hydrophobic guests, functional molecular motifs may also be introduced through covalent integration within the macromolecular structure.[50, 167-169] Indeed, the incorporation of photoactive functionalities within micellar supramolecular assemblies has shown great promise as a new strategy for the creation of nanosized photonic devices and fluorescent probes with photoresponsive emission characteristics.[8, 36, 74, 75, 135, 170, 171] In contrast to the previously discussed covalent supramolecular photochrome-fluorophore dyads/triads (chapter 4), which often require a great deal of synthetic effort, the introduction of photoresponsive units within the supramolecular micelle-constructs is much more straightforward. Given the self-assembly and modular nature of these architectures, they allow for the convenient integration of various photochromic and fluorescent components. The average donor-acceptor separation can be altered by varying the ingoing concentrations and, consequently, enabling tuning of intermolecular electron and/or energy transfer reaction rates. Furthermore, the micellar approach enables the operation of organic photochromic molecules in aqueous solution. It is not uncommon that photochromic compounds, which exhibit excellent switching performance in organic solvents, experience reduced switching capability, as well as possible solubility issues, when introduced to more polar solvents.[172, 173]

In terms of establishing FRET communication between a donor-acceptor pair, the easiest way to achieve this is by a “cocktail approach”. In essence, by dissolving both donor and acceptor together in high concentration, ~0.1M, the resulting average donor-acceptor distance becomes ~25 Å. This is well within the Förster distance of most common efficient FRET-pairs. However, assuming solubility is not an issue, this approach will typically result in extreme optical densities and significant inner filter effects. Similarly, the micellar approach permits the creation of nanosized hydrophobic environments with localized high-concentration “cocktails” of photoactive molecules, while still rendering the total “bulk” absorption low and thus enabling photophysical characterization.

In paper IV, the micellar approach has been used to create photochromic supramolecular constructs which enable dichromatic emission-color tuning by photoswitching of energy transfer between a 9,10-diphenylanthracene donor and a fluorescent diarylethene photoswitch.

7. Original Work

7.1 Paper I – An all-photonic molecular D-flip flop

In circuitry for information processing, different memory storage units such as flip-flops, latches, and switches are used in order to retain data in between operating cycles. The simplest circuit is the Set-Reset (SR) latch, which provides two input and one single output. By application of the Set input, the output becomes 1. The output remains unchanged until Reset is applied, and then the output becomes 0. The SR latch is event-triggered, meaning that it changes state instantaneously in response to changes in input signal and this is achieved through the cross-coupling and signal feedback two NOR gates. A flip-flop, on the other hand, refers to a gated latch, which requires the triggering of a clock signal to enable a change of state.

One such circuit is the D-flip flop. The D refers to *delay/data* and it is the most commonly used flip-flop in silicon circuitry. The circuit has two input signals, *In* and *Clock*, and two complementary output signals Q and Q' . *In* supplies the information to be stored by the circuit and *Clock* is used to trigger "listening" by the memory element. Simply, to induce a change of state, *Clock* must be applied to prime the memory element to "listen" and at any time when *Clock* is applied, the system output Q will adapt the state of *In*. When *Clock* is withdrawn, the output Q of the D flip-flop will remain unchanged until once again triggered by *Clock*. In light of this, a specific digital signal can be recorded and saved. In conventional silicon circuitry the D-flip flop is achieved by combination of four NAND gates and one NOT gate (Figure 17).

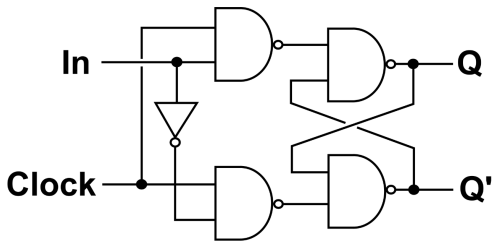

Clock (532 nm)	*In* (1064 nm)	$Q_{current}$ (644 nm fluo)	Q_{next} (644 nm fluo)
0	0	0	0 (0.087)
0	0	1	1 (0.91)
0	1	0	0 (0.097)
0	1	1	1 (0.90)
1	0	0	0 (0.087)
1	0	1	0 (0.087)
1	1	0	1 (0.91)
1	1	1	1 (0.91)

Figure 17. Left: Logic diagram of D-flip flop. The diagram shows the electronic representation of the integration of four NAND gates and one NOT gate with feedback loops. Right: Truth-table of D-flip flop.

This paper involves the realization of an all-photonic molecular D flop-flop by using a photochromic fulgimide in combination with non-linear (SHG/THG) crystals. In essence, the fulgimide **1** functions as the memory retention unit and the light operations with non-linear crystals implicate the combinational logic enabling selective data storage. During operations with light, the fulgimide undergoes reversible photochromic switching. By harnessing the fluorescence of the closed-form, photonic read-out of state is enabled. The fulgimide exists in two open conformers, **1E** and **1Z**, and their interconversion can promoted by exposure to UV-light. Irradiation with UV-light in addition induces the 6π-photocyclization reaction, proceeding from the open E-form, which yields the closed-form **1C** (Figure 18, right).

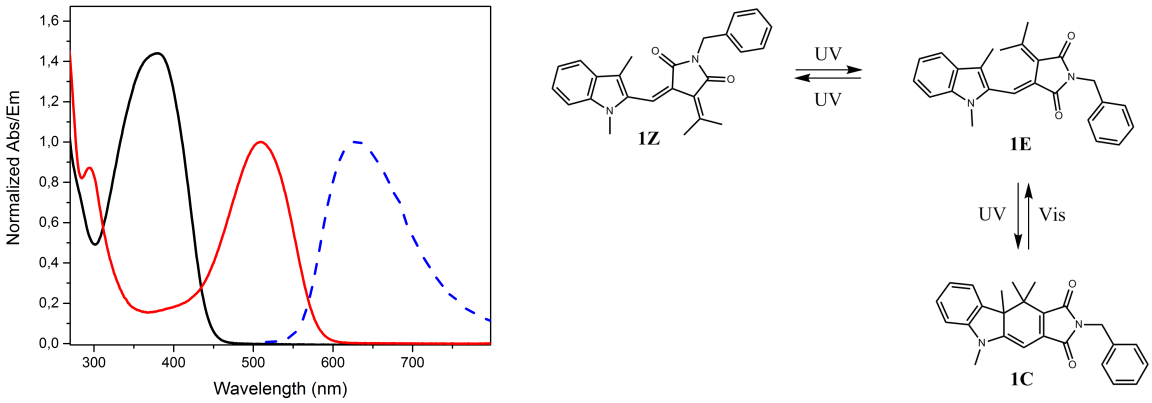

Figure 18. Left: Absorbance spectra of **1E** (black solid), **1C** (red solid) and emission spectrum of **1C** (blue dashed). Right: Structure and interconversion scheme of **1Z**, **1E** and **1C**.

In acetonitrile, the **1E** displays an absorption peak at 374 nm (Figure 18, left). Exposure to 365 nm UV-light for 4 min results in the photoinduced ring-closure to **1C** ($\phi_{iso,E\rightarrow C} = 0.13$) with associated coloration as well as the appearance of a bathochromic absorption band at 523 nm. In the photostationary state, virtually 100% was isomerized into **1C** and was confirmed by ^{1}H NMR. Due to the simultaneous UV-induced E↔Z interconversion, three components are present during the photoinduced generation of **1C** and therefore, no isosbestic point is observed in the absorption spectra monitoring the coloration reaction. The reverse ring-opening reaction was promoted by irradiation with visible light (40 s). In this case, however, as only the two species **1C** and **1E** are present during the photoisomerization, indeed an isosbestic point is observed.

The signal modulation is implicated by the combination of second-harmonic generation (SHG) and third-harmonic-generation (THG) crystals (Scheme 3). Data input *In* is defined as the fundamental wavelength of an Nd:YAG laser, 1064 nm IR-light, and *Clock* as 532 nm visible light produced through an SHG crystal. The simultaneous application of *In* and *Clock*, that is, the combination of 1064 nm and 532 nm, results in the generation of 355 nm light *via* the THG crystal. It is noteworthy that neither **1Z**, **1E**, nor **1C** absorb light of 1064 nm. When applied in the photochromic switching of fulgimide **1**, a number of cases arise:

i) Without the application of IR or visible light (*In* = *Clock* = 0), no change occurs and the photochromic state remains unchanged ($Q_{current} = Q_{next}$).

ii) Similarly, in the application of IR light (*In* = 1) without the presence of visible light (*Clock*=0), neither absorption of IR-light nor generation of UV-light takes place, and the photochromic state remains unchanged ($Q_{current} = Q_{next}$).

iii) Application of only visible light (*Clock* = 1) without the presence of IR light (*In* = 0) will result in the non-fluorescent open-form E-isomer ($Q_{next} = 0$) regardless of the previous state of the photochromic fulgimide. If previously in the closed-form

($Q_{current}$ = 1), absorption of the green light will trigger the ring-opening into the E-form (Q_{next} = 0) and if already in the open E-form, no absorption takes place and the system remains unchanged ($Q_{current}$ = Q_{next} = 0).

iv) In simultaneous application of IR-light and visible light (*In* = *Clock* = 1), UV-light of 355 nm is generated via the third-harmonic generating crystal and will convert **1C** into **1E** with concomitant decrease in fluorescence emission and output (Q_{next} = 0).

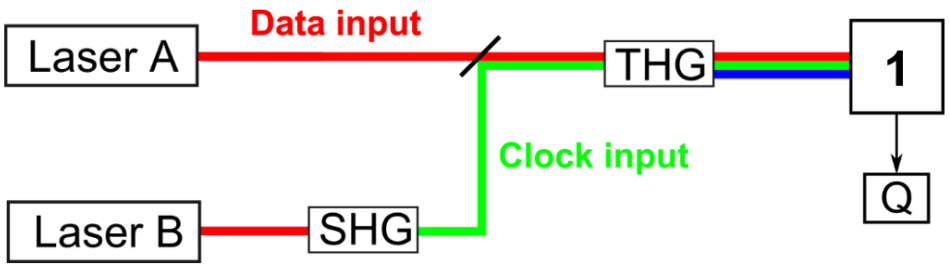

Scheme 3. Schematic representation of the experimental setup for the implication of a D-Flip Flop with fulgimide **1**, non-linear crystals (SHG and THG) and Nd:YAG lasers A and B.

If utilized in real-life information storage application, a memory storage unit must be able to perform multiple read/write cycles as well as long-time storage. Thus, to investigate the fatigue resistance to photonic stimuli, an experiment of 10 switching cycles was undertaken and no noticeable degradation was observed. Furthermore, the high thermal stability of both **1E** and **1C** (no significant changes after 10 days in the dark) provides the possibility for long-term storage, leaving the state of the system unchanged, unless subjected to photonic stimuli. As the implication of the D-flop flop is fully photonic in nature, no chemical inputs are needed. As such the system does not experience any limitations in terms of diffusion-controlled reactivity or buildup of chemical waste. The intrinsic switching time of photochromic fulgimides are typically on the time-scale of less than 10 ps, which translates into a theoretical switching rate of 100 GHz. However, as the system operates as a micromolar range ensemble, 45 s irradiation was needed to switch the entire population. The presented system is an obvious demonstration of proof-of-concept, not intended to compete with currently available silicon-based technology in terms of performance. However, it does indeed show the functional integration of a complex logic circuit, which in conventional silicon circuitry requires the physical integration of multiple logic gates (NAND and NOT) and the incorporation cross-coupled feedback loops. A remaining challenge is found in the concatenation of multiple molecular logic elements and their integration into larger logic circuits and networks. As the operation of this system is all-photonic, the issues regarding input/output inhomogeneity is formally overcome. However, the energetic difference of the output (644 nm) and input (355 nm) signals still remain an issue. Furthermore, the omnidirectional nature of the emission of light poses a problem in terms of concatenation and achieving individually addressable molecular logic gates.

In conclusion, we have realized an all-photonic molecular D-flip flop using photochromic fulgimide **1** in combination with non-linear crystals and Nd:YAG lasers. In essence, the photochromic fulgimide **1** provides the memory storage functionality and fluorescence read-out, while the combination of SHG/THG crystals are used to implicate the clock-gated logic behavior of the D-flip flop truth-table. Even though the presented system does not offer much in terms of real-life application, it clearly illustrates the promises held by photochromic entities for molecular information processing and storage. However, reaching the full potential in this regard, indeed requires the gate-specific addressability and communication between distinct molecules. Although this may seem farfetched in the near future, it stands to reason that continuous investigation into alternative logic platforms, fruitful or not, is necessary for the development of future information processing technologies. Finally, on a personal note, I believe that the future technologies and the next paradigm shift is to be found in either photonic or quantum-based devices.

7.2 An All-Photonic Molecule-Based Parity Generator/Checker for Error Detection in Data Transmission

In digital data transmission it is desirable to ensure that communication proceeds in a satisfactory manner and that no distortion of data occurs. One way to achieve this is by using the combination of a parity generator and checker. The parity generator creates a control digit, a parity (P) bit, by comparing the relationship of the two incoming data signals, D_1 and D_2. The control digit P is then transmitted alongside D_1 and D_2 to the transmission end-point and the parity checker. Here, the received data signals D_1 and D_2 are again compared to generate a second parity bit P′ which in turn is compared to the initial parity bit P. If both parity bits are equal, P = P′, it can be concluded that the transmission ensued without distortion. This is represented as output C = 0. If, on the other hand P ≠ P′, the data transmission has been altered along the way and is indicated by output C = 1.

The function of the parity generator/checker in conventional silicon circuitry is implicated by the total combination of three exclusive OR (XOR) logic gates (Figure 19, top). The 2-bit XOR gate is the logic element of each comparative operation and generates output P = 0 if the two inputs D_1 and D_2 are equal. When inputs D_1 and D_2 are different, the output is P=1. The final XOR-element compares the generated parity bits P and P′ and gives the output C. The corresponding truth-table is shown in Figure 19 (bottom).

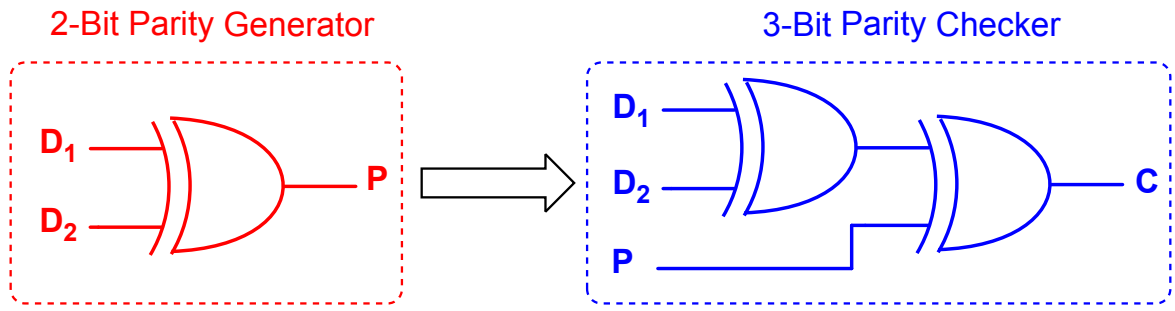

entry	inputs		output
	$D_1{}^b$	$D_2{}^b$	P^c
1	0	0	0
2	0	1	1
3	1	0	1
4	1	1	0

Figure 19. Top: Logic scheme of integrated XOR-gates implicating parity generation/checking. Bottom: Truth-table of XOR-gate.

In order to implicate the desired XOR behavior, two triadic photochromic systems exhibiting *off-on-off* fluorescence in response to UV-exposure were used. A fulgimide (**FG**) derivative and a dithienylethene (**DTE**) derivate were conjugated through a common trisubstituted phenyl ring. Triad 1 consists of two **FG** units and one **DTE** unit whereas Triad 2 consists of one **FG** and two **DTE** units (Figure 20). It is important to note that only the closed-form of the fulgimide $\mathbf{FG_c}$ is fluorescent ($\lambda_{f,max}$ = 630 nm, τ_f = 135 ps, ϕ_f = 0.005) and that the spectral overlap of **DTEc** absorption with $\mathbf{FG_c}$ emission results in FRET-based quenching of the $\mathbf{FG_c}$ excited-state and regulation of the fluorescence emission.

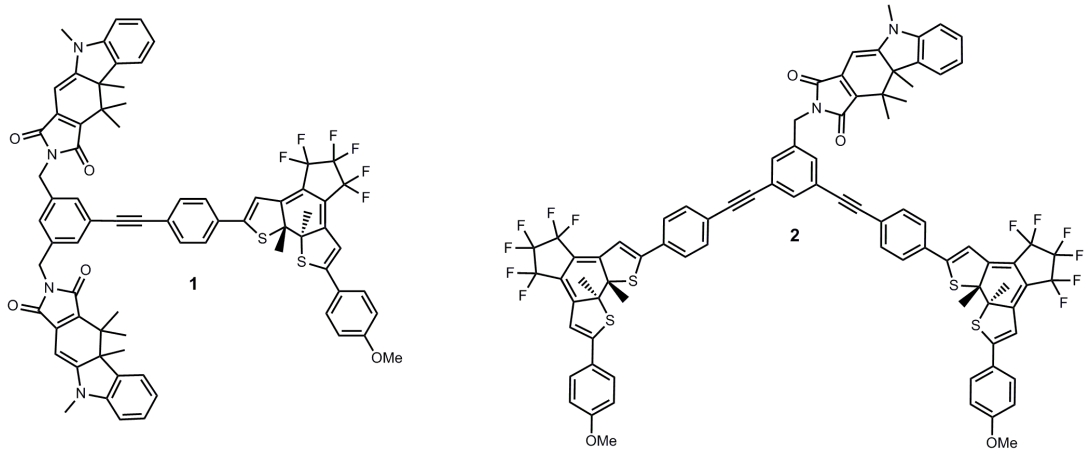

Figure 20. Molecular structure of triad **1** and triad **2**, both shown in the fully closed $\mathbf{FG_c}$-$\mathbf{DTE_c}$ state.

In the initial state, $\mathbf{FG_o}$-$\mathbf{DTE_o}$, no fluorescence is observed. Exposure to UV-light induces the photogeneration of both $\mathbf{FG_c}$ and $\mathbf{DTE_c}$. However, as the ring-closing reaction to yield $\mathbf{FG_c}$ is faster (time constant 312 s) than the generation of $\mathbf{DTE_c}$ (time constant 730 s), the irradiation results in an initial build-up of the $\mathbf{FG_c}$-$\mathbf{DTE_o}$ state with a corresponding rise in fluorescence emission. As the population of molecules in the $\mathbf{FG_c}$-$\mathbf{DTE_c}$ state increases, the fluorescence intensity reaches a plateau and subsequent decay as FRET-based quenching of $\mathbf{FG_c}$ by $\mathbf{DTE_c}$ becomes more and more predominant. The system is reversed to $\mathbf{FG_o}$-$\mathbf{DTE_o}$ by irradiation with visible light. The isomerization between all the implicated forms is shown in Figure 21 (left).

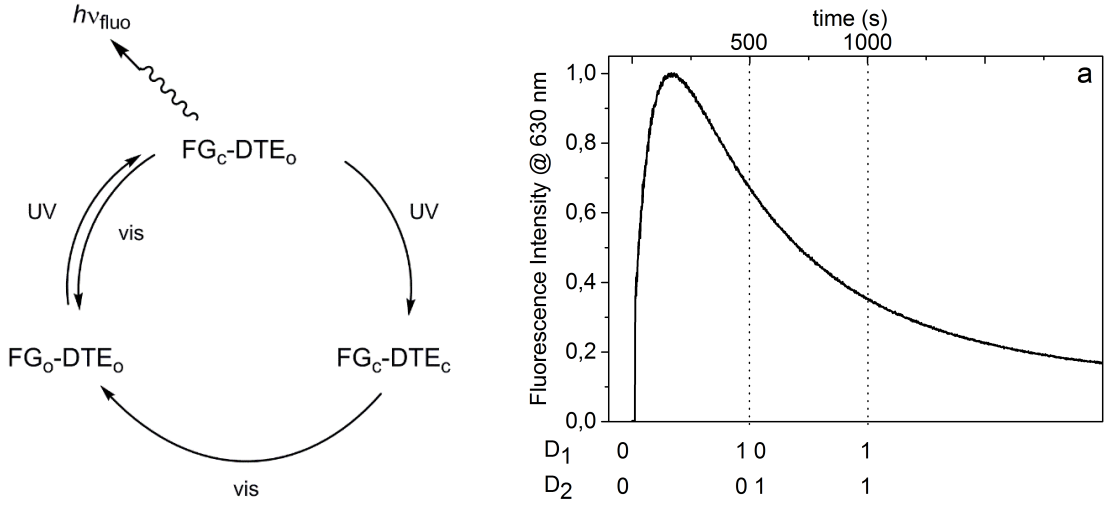

Figure 21. Left: Isomerization scheme showing the photoinduced interconversion between **FG$_o$-DTE$_o$**, **FG$_c$-DTE$_o$** and **FG$_c$-DTE$_c$**. Right: Fluorescence response of triad **1** under steady irradiation with 380 nm UV-light (0.5 mW/cm^2). The dotted lines at 500s and 1000s indicate one and two "doses" of UV-light.

The realization of the displayed "neuron-like" *off-on-off* fluorescence response is not trivial and requires the fulfillment of a number of design criteria to be realized and ensure optimal performance. Firstly, the initial state must be non-fluorescent and the photoinduced isomerization must proceed through a fluorescent intermediate, which upon subsequent irradiation is rendered non-fluorescent. Secondly, as the emission proceeds from the closed-form **FG$_c$**, it is essential that the generation of **FG$_c$** is indeed more rapid than the generation of **DTE$_c$** as to avoid premature quenching of the generated **FG$_c$** units, which may suppress or even eliminate the intended rise in emission intensity. On the other hand, in order to maximize the final quenching and fluorescence turn-off, the population at the photostationary state should involve as much **DTE$_c$** as possible.

The implementation of the 2-bit parity generator, corresponding to the abovementioned XOR logic, was achieved by defining output P as the fluorescence intensity of **FG$_c$** at 630 nm and input data D_1 and D_2 both as the degenerate input of 380 nm light (0.5 mW/cm^2). Initially, the system is in the non-fluorescent **FG$_o$-DTE$_o$** form and the fluorescence output P=0. Upon exposure to one dose of UV-light (D_1 or D_2 = 1) enriches **FG$_c$-DTE$_o$** and turns on fluorescence emission (P = 1). However, additional exposure to UV-light ($D_1 = D_2 = 1$) only further advances the ring-closure to **DTE$_c$** and generates the non-fluorescent **FG$_c$-DTE$_c$** (P = 0). The corresponding time-based fluorescence response of Triad **1** is shown in Figure 21 (right). Triads 1 and 2 was also used for the implication of a 3-bit parity checker. The corresponding truth-table is shown in Table 1.

	inputs			output	
entry	D_1	D_2	P	C	Interpretation
1	0	0	0	0	ok
2	0	1	0	1	error
3	1	0	0	1	error
4	1	1	0	0	ok
5	0	0	1	1	error
6	0	1	1	0	ok
7	1	0	1	0	ok
8	1	1	1	1	error

Table 1. Truth-table of 3-bit parity generator with P=0 exhibiting XOR logic (1-4) and P=1 exhibiting XNOR logic (5-8).

The realization of a 3-bit parity checker can be divided into two parts: P = 0 or P = 1. The case where P = 0 corresponds to XOR logic (with respect to D_1 and D_2) and fluorescence intensity represents the output C. The case of P = 1 instead represents the complementary XNOR logic (with respect to D_1 and D_2). As the XOR logic has already been implemented and described above, the focus is now shifted to the XNOR logic. In comparison to the XOR logic, the implication of XNOR logic with the photochromic triads is less straight forward and requires reassignment of the input definitions. Here, D_1 is visible light ($\lambda > 540$ nm) while P and D_2 are defined as degenerate 380 nm UV-light. In addition, the inputs P, D_1 and D_2 must be applied sequentially in the string P-D_1-D_2, to account for the inherent memory functionality of the thermally stable photochromic triads. Once again, the initial state is **FG_o-DTE_o** and application of P alone (one UV dose) results in the generation of the fluorescent **FG_c-DTE_o** and output C = 1. Additional application of UV-light (D_2 = P = 1) pushes the distribution towards the non-fluorescent **FG_c-DTE_c**, providing output C = 0. Alternatively, application of P followed by D_1 (visible light) brings the system back to the original non-fluorescent **FG_o-DTE_o** state and output C = 0. On the application of all inputs (P = D_1 = D_2 = 1), the system is finally placed in the fluorescent **FG_c-DTE_o** state with output C = 1.

The corresponding fluorescence responses for the implication of XOR logic (1–4) and XNOR logic (5–8) for triad **1** are shown in the bar diagram in Figure 22 (left).

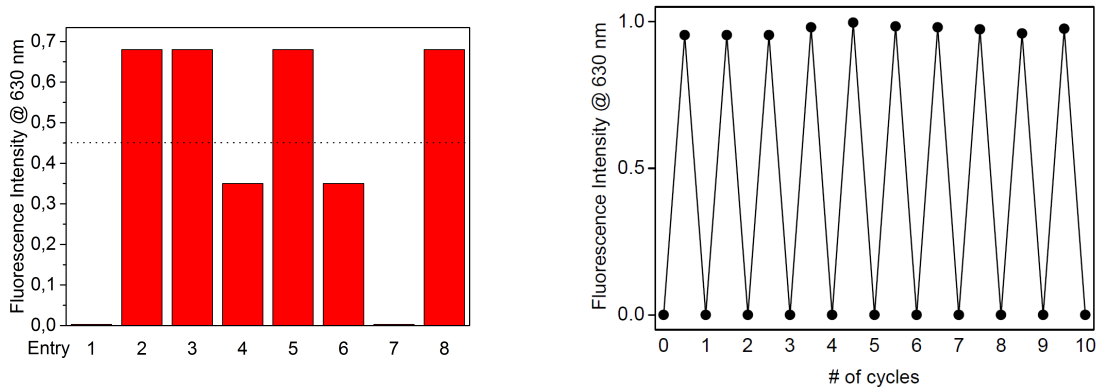

Figure 22. Left: Performance of XOR (1–4) and XNOR (5–8) logic operations with corresponding fluorescence response for triad **1**. Dotted line indicated the threshold value (0.45) for the assignment of binary 0 and 1. Right: Repeated switching of triad **1**. Each cycle starts in the **FG$_o$-DTE$_o$** form and involves UV irradiation at 380 nm (240 s) followed by visible light (λ > 540 nm) irradiation (30 min).

In addition to the implication of the parity generator/checker functionality, the fatigue resistance (i.e. robustness of multiple switching operations) as well as thermal stability of the Triads 1 and 2 were evaluated. Alternate irradiation with UV and visible light induced cyclic switching between the **FG$_o$-DTE$_o$** and **FG$_c$-DTE$_o$** states and was monitored by fluorescence emission. The results indicate no significant loss in fluorescence emission over at least 10 operation cycles (Figure 22, right). Furthermore, all species exhibit high thermal stability (< 10% variation in absorption spectra of **FG$_c$-DTE$_c$** after one week in the dark).

In summary, paper II demonstrates the proof-of-principle implication of both 2-bit parity generation and 3-bit parity checking in terms of all-photonic molecular XOR and XNOR logic with the photochromic Triads 1 and 2. The achieved "neuron-like" *off-on-off* fluorescence response indeed indicates the successful realization of the intended function and the fulfillment of the essential design parameters. The implication of the XOR-gate is intuitive and straight forward, whereas the realization of the XNOR logic behavior of the 3-bit parity checker requires the redefinition of input signals and the imposed condition of sequential application.

7.3 Reversible Energy-Transfer Switching on a DNA Scaffold

In the field of DNA photonics, sequence specific base-pairing and hybridization into double-stranded DNA helices is used to enable the precise spatial organization of chromophores and creation of self-assembled architectures of higher order complexity. Early examples includes photonic DNA wires, which realize long-distance energy-transfer by hybridization of multiple fluorophore-modified ss-DNA oligos onto a common template strand.[67, 68] However, due to the irreversible nature of the achieved FRET-mediation in these constructs, reversible switching of the photonic flow of energy is not possible.

In this paper, we show the realization of photochromic switching of the DNA-binding of a spiropyran derivative and the implication of reversible gating of excitation energy flow on a DNA template. As previous studies have shown,[27, 111] the affinity for DNA-binding of photochromic spiropyran is significantly enhanced upon UV-induced transformation into the ring-open merocyanine form (**MC**). During this transformation, the two orthogonally oriented heterocycles of the closed-form isomer of spiropyran (**SP**) undergo planarization, and thus provide an excellent motif for DNA-binding by intercalation. Furthermore, the isomerization involves an associated bathochromic shift in absorption, due to the extended π-conjugated system in the merocyanine isomeric form. These two properties combined (the concommitant alteration in DNA-binding affinity and spectral shift in absorption) enable the reversible photochromic gating of energy-transfer of a FRET donor-acceptor pair positioned on a DNA-scaffold.

The selected spiropyran for this study was the amidine-substituted derivative **1SP**, which undergoes the photoinduced ring-opening reaction to yield merocyanine **1MC** ($\phi_{iso} = 0.02 \pm 0.01$) upon exposure to UV-light (254 nm). The reverse reaction is induced by irradiation with visible light ($\lambda > 450$ nm). Furthermore, **1SP** and **1MC** interconvert thermally and in the dark, a thermal equilibrium with a 20/80 [**1SP**]/[**1MC**] ratio is established (time constant ~6 h at room temperature). Protonation of the phenolate oxygen of merocyanine yields **1MCH**$^+$ (pK_a of 5.2). In addition, **1MCH**$^+$ is reversed to **1SP** under the irradiation of visible light. Upon DNA-binding, the pK_a of **1MCH**$^+$ is increased to a pK_a = 6.8. As the DNA-binding affinity of **1MCH**$^+$ ($K = 3.4\times10^4\ M^{-1}$) is 35 times higher than that of **1MC** (likely due to the increased electrostatic attraction to the phosphate backbone), the experiments were performed at acidic conditions (pH = 5.4), making **1MCH**$^+$ the dominant DNA-binder. The three forms **1SP**, **1MC** and **1MCH**$^+$ with interconversion pathways are shown in scheme 4.

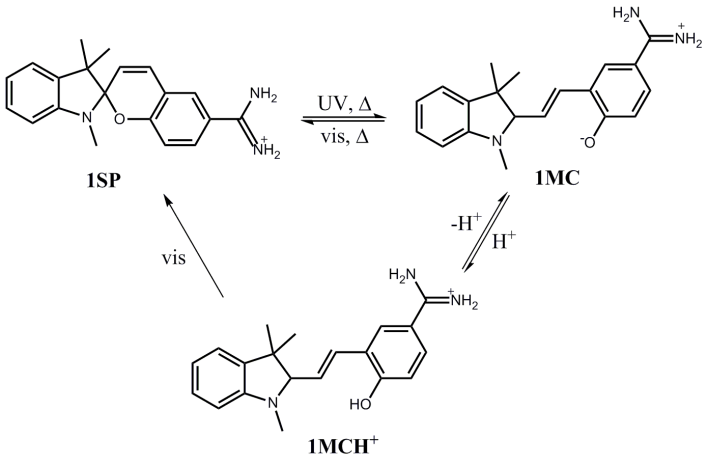

Scheme 4. Structures and interconversion pathways of **1SP**, **1MC** and **1MCH**$^+$.

The DNA scaffold consists of two complementary 20-mer ss-DNA oligos, **OPB** and **OA488**, with covalently attached fluorophores Pacific Blue (**PB**) and Alexa 488 (**A488**). Together, **PB** and **A488** form a donor-acceptor pair for FRET, with R_0 theoretically calculated to equal 52 Å (assuming κ^2=2/3). The corresponding calculated R_0 of the **PB-MCH**$^+$ pair is 38 Å. The implicated absorption and emission spectra of **PB, A488** and **1MCH**$^+$ can be seen in Figure 23 and illustrates the spectral overlap of the **PB** emission with the absorption spectra of the two different FRET acceptors.

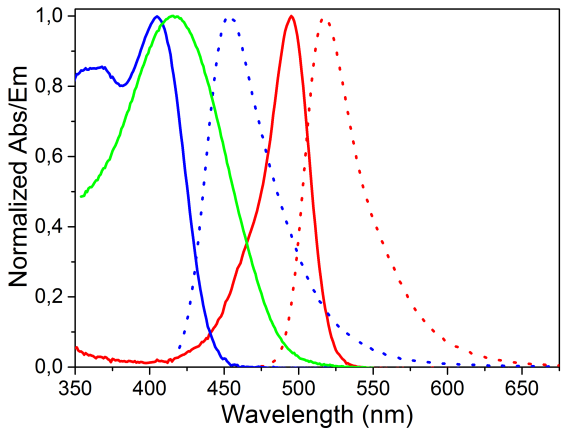

Figure 23. Absorption (solid lines) and emission (dotted lines) of **OPB** (blue) and **OA488** (red) hybridized to their respective unlabeled complementary single-strand, and the absorption spectrum of **1MCH**$^+$ (green) bound to DNA.

The two single-strands, **OPB** and **OA488**, are hybridized to yield a DNA double helix (Scheme 5), which positions **PB** nine base-pairs away from **A488**, corresponding to a donor-acceptor distance of ~ 31 Å. FRET communication between **PB** and **A488** is established and, as the **1SP** form shows no detectable DNA-binding, energy-transfer proceeds unimpeded between **PB** and **A488**. However, UV-irradiation yields **1MCH**$^+$, which intercalates with the DNA-scaffold and

in turn, terminates **PB-A488** communication by competitive deactivation of excited-state **PB** through FRET-sensitization of **1MCH**$^+$.

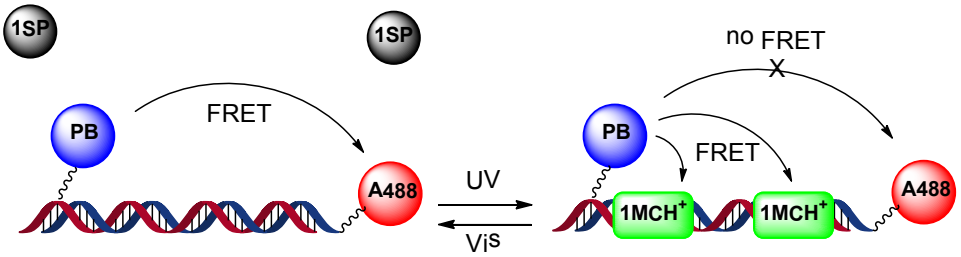

OPB: 5'-GCCGAT**PB**GTGGTCGGAGAGA

OA488: 5'-TCTC**A488**CCGACCACAATCGGC

Scheme 5. a) Schematic representation of the fluorophore appended DNA double helix displaying photoinduced interconversion of **1SP**↔ **1MCH**$^+$ enabling reversible *on–off* switching of FRET between **PB** and **A488**. b) Base-sequence of the **OPB** and **OA488** oligonucleotides.

The DNA oligos, **OPB** and **OA448**, were hybridized with each other, as well as with their respective unlabeled complementary single-strands, to yield three samples of ds-DNA. The corresponding fluorescence spectra are shown in Figure 24.

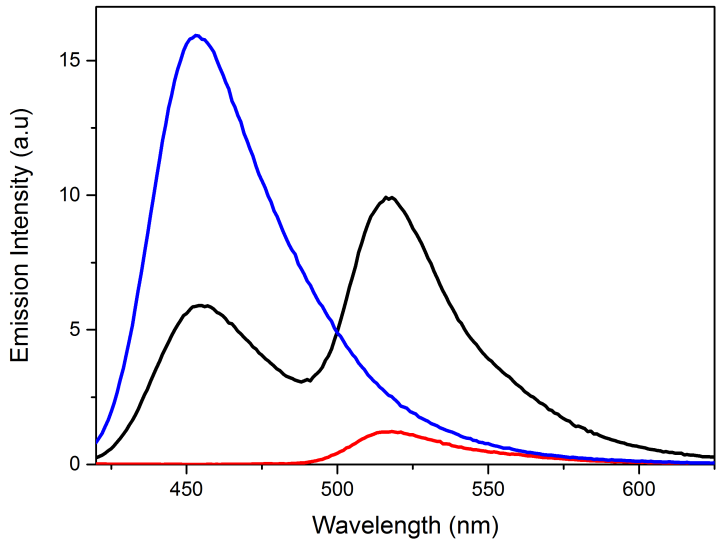

Figure 24. Fluorescence emission spectra (λ_{ex}=410 nm) of **OPB** (blue), **OA488** (red), and the **OPB-OA488** (black) double-strand.

To ensure the complete hybridization of all **OA488** strands (1µM), **OPB** was used in a 1.2-fold excess (1.2µM). The corresponding emission spectrum of the **OPB-OA488** double strand clearly shows the quenching of **PB** with concomitant sensitization of **A488**. Taking into account

the emission arising from the 1.2-fold excess of the **OPB** strand, as well as the minor component of direct excitation observed for **OA488**, the FRET efficiency between **PB** and **A488** was estimated to equal 78%. Furthermore, quenching of the **PB** excited-state was confirmed by complementary TR-SPC measurements. The lifetime of **PB** in **OPB** hybridized with the unlabeled complementary strand was 3.4 ns, as opposed to the heavily quenched lifetime of 0.62 ns observed for the **OPB-OA488** double strand. Corresponding to an 82% quenching efficiency, the results are in excellent agreement with the steady-state fluorescence measurements. Given the calculated Förster distance of 52 Å and the donor-acceptor separation of 31 Å, a FRET efficiency of 96% was expected. The discrepancy is tentatively explained as a deviation from the assumed $\kappa^2=2/3$ — likely due to restrictions in free rotation imposed by the fluorophore-DNA linkers.

While it was hypothesized that **1SP** would be completely inactive in terms of intermolecular quenching reactions, the introduction of **1SP** (25µM) to the double-strand **OPB-OA488** resulted in decreased emission intensity (Figure 25, black vs green line) of both **PB** and **A488.** This unexpected decrease is assigned to a weak static quenching complex between **1SP** and **PB**, which is based on the fact that no-short lived component was observed in the TR-SPC fluorescence decay. Furthermore, in the presence **1SP** the observed emission intensity of **OPB-OA488** changed over time, indicating that the thermal generation of **1MCH**$^+$ from **1SP** is too slow to explain the quenching arising from the addition of **1SP** (see supporting information, Figure S3). In addition, variations in emission intensity with varying total concentration of **1** at thermal equilibrium (1–25µM), shows that the initial quenching from addition of 25 µM **1SP** is equivalent to ~ 5µM **1MC**/**1MCH**$^+$. Hence, quenching *via* residual amounts of **1MCH**$^+$, either from thermal generation or from incomplete isomerization to **1SP** in the stock solution, could be excluded.

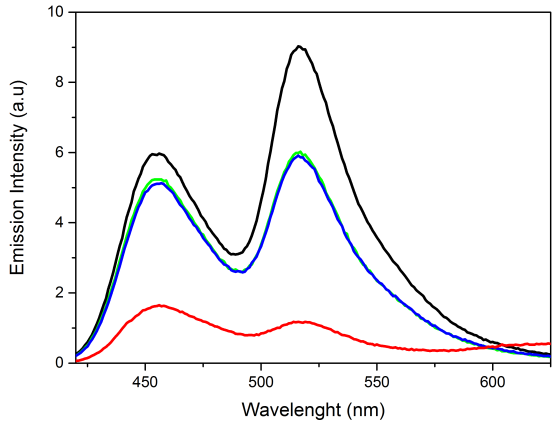

Figure 25. Fluorescence emission spectra (λ_{ex}=410 nm) of **OPB-OA488** double-strand prior to (black line) and after (green line) addition of 25 µM **1SP**. The red line shows the emission intensity after 2 min. UV (254 nm) to yield the DNA-binding **1MC** and **1MCH**$^+$, resulting in quenching of the **PB** and **A488** emission intensities. The blue line shows the recovery in emission intensity after subsequent visible light irradiation (5 min, $\lambda > 450$ nm) to trigger the reverse isomerization to **1SP**.

Upon exposure to UV-light (254 nm) for 2 min (red line), the DNA-binding species **1MCH**$^+$ is generated, resulting in additional quenching of the emission intensity of **PB** with concomitant decrease in sensitization of **A488**. This result indeed supports the expected interruption of **PB**-**A488** FRET-communication by DNA-bound **1MCH**$^+$. After subsequent irradiation with visible light to induce ring-closure to **1SP**, the initial emission intensity is recovered and thus confirm the reversibility of the energy-transfer switching.

In order to further investigate the FRET efficiency between **PB** and **1MCH**$^+$, TR-SPC measurements were performed. The experiment showed that the **PB** excited-state is too efficiently quenched for the lifetime to be resolved, that is, as it is significantly shorter than the IRF ~40 ps. Given the concentration of **1MCH**$^+$, the number of DNA binding sites, and the DNA-binding affinity of **1MCH**$^+$ ($K = 3.4\times10^4\ M^{-1}$), an average distance of four base-pairs between DNA-bound **1MCH**$^+$ and **PB** is expected. With an R_0 of 38 Å for the interaction of DNA-bound **1MCH**$^+$ and **PB**, the estimated DNA-binding density will quench the lifetime of **PB** to 7 ps or shorter. Hence, the residual **PB** and **A488** emission are successfully accounted for by the 1.2-fold excess **OPB** single-strands and the direct excitation of **A488**.

Furthermore, at very high binding densities, photoinduced electron transfer (PET) between **PB** and **1MCH**$^+$ cannot be excluded. Experiments with single-strands of **OPB** showed that **1MCH**$^+$ induces **PB** emission quenching, however, to a much lesser extent. In addition, the PET driving force has not be evaluated due to the absence of redox potentials.

In conclusion, the photoinduced generation of **1MCH**$^+$ from **1SP** enables complete deactivation of the FRET process between **PB** and **A488**. Exposure to visible light triggers the back-isomerization to **1SP** and restores the emission intensities of **PB** and **A488** to their original values. Hence, the photo-controlled interconversion of **1SP** and **1MCH**+ successfully achieves the reversible gating of the **PB** and **A488** FRET process.

7.4 Paper IV - Emission Color-Tuning and White Light generation

In this paper, we present the realization of photo-controlled FRET-based emission color-tuning and white-light generation by utilizing a photochromic multi-component donor-acceptor system. This system consists of a fluorescent donor 9,10-diphenylanthracene (**DPA)** and a photochromic diarylethene acceptor (**DAE)** encapsulated in the lipophilic core of self-assembled micellar nano-constructs formed by amphiphilic copolymers in aqueous solution.

The open-form of the acceptor, **DAE$_o$**, is non-fluorescent and has no spectral overlap with the emission of the donor **DPA**. Irradiation of **DAE$_o$** with ultraviolet light (254 nm) induces ring-closure to yield the fluorescent closed-form **DAE$_c$** (ϕ_{iso}=0.42), which is accompanied by a red-shift in the absorption spectrum, positioning the absorption of the closed-form **DAE$_c$** in spectral overlap with the emission of donor **DPA**. The reverse isomerization is achieved through irradiation with visible light (λ=523 nm). The absorption and emission spectra of all implicated forms are shown in Figure 26.

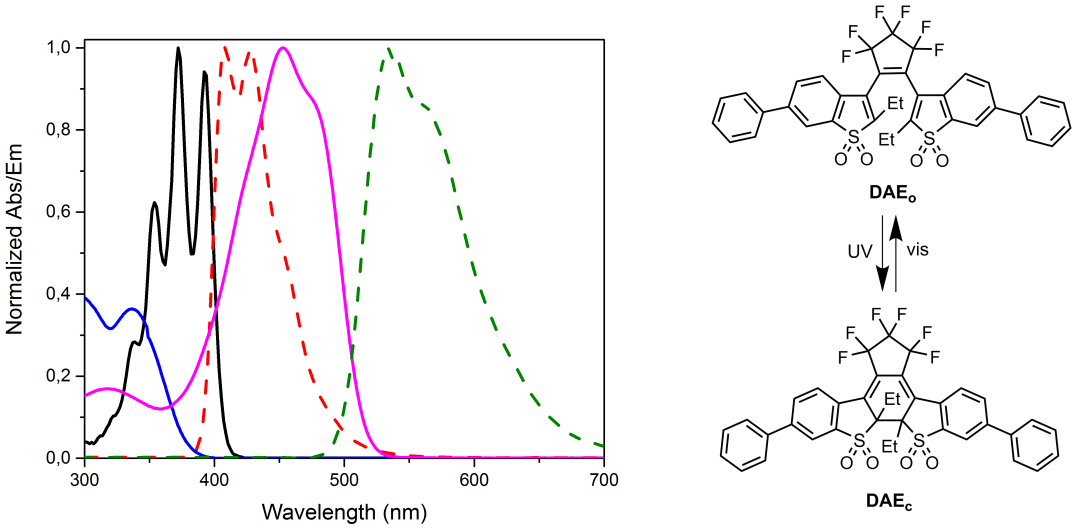

Figure 26. Left: Normalized absorption of **DAE$_o$** (blue solid line), **DAE$_c$** (magenta solid line) and **DPA** (black solid line), as well as fluorescence emission spectra of **DPA** (red dashed line) and **DAE$_o$** (green dashed) in AcCN. The red dashed line and the magenta solid line illustrate the overlap between **DPA** donor emission and **DAE$_c$** absorption. Right: Structure and photoinduced interconversion of **DAE**.

The overlap integral between **DPA** emission and **DAE$_c$** absorption is significant (R_0 = 52 Å in acetonitrile) and enables FRET communication from the excited-state fluorophore to the closed-form acceptor. As the overlap between open-form **DAE$_o$** absorption and **DPA** emission is non-existent, FRET will exclusively proceed to **DAE$_c$.** Being highly hydrophobic, both **DPA** and **DAE** are essentially insoluble in water. However, upon hydration in the presence of amphiphilic co-polymer **ST-7-4**, polymer micelle formation is encouraged and effectively encapsulates both **DPA** and **DAE** in close proximity inside the hydrophilic core (see Scheme 6).[8] Dynamic light scattering (DLS) measurements of the formed micellar aggregates show an

average hydrodynamic diameter of 15 nm. In addition, both **DPA** and **DAE** retain their photophysical properties upon encapsulation within the micelles, aside from a small bathochromic shift (~ 2–5 nm) in emission and absorption spectra. The fluorescence quantum yields of both donor **DPA** (ϕ_{em} = 1) and acceptor **DAE$_c$** (ϕ_{em} = 0.75) was determined to be unaffected upon encapsulation.

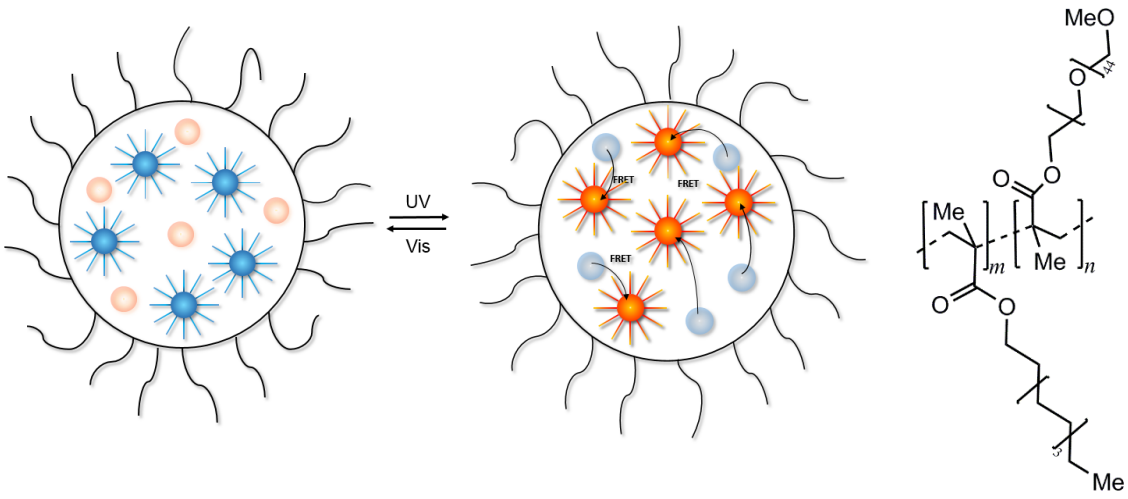

Scheme 6. Left: Schematic representation of donor **DPA** and acceptor **DAE** encapsulated in polymer micelles. As the acceptor is in the non-florescent open-form **DAE$_o$**, FRET is inactive and the blue donor emission dominates. Irradiation with UV-light induces formation of fluorescent closed-form **DAEc**, which activates FRET communication between donor and acceptor and renders the acceptor emission dominant. Right: Molecular structure of amphiphilic polymer **ST-7-4**.

Initially, the photochromic acceptor is present in the open-form **DAE$_o$**, therefore energy-transfer is not observed and fluorescence is dominated by the blue emission component adhering to the donor **DPA** (Figure 27). However, upon UV-irradiation **DAE$_o$** isomerizes into the fluorescent **DAE$_c$** and spectral overlap is established between **DPA** emission and **DAE$_c$** absorption — activating FRET communication. The emission from the excited-state donor **DPA** is therefore quenched through energy-transfer with concomitant sensitization and emission of excited-state **DAE$_c$.** Thus, as the interconversion from **DAE$_o$** to **DAE$_c$** proceeds, the concentration of **DAE$_c$** increases and reduces the average between **DPA** and **DAE$_c$** distance while simultaneously increasing the number of possible FRET acceptors. Consequently, the overall FRET efficiency is increased, resulting in a gradual decrease of **DPA** emission and a concomitant increase of sensitized **DAE$_c$** emission. Hence, the emission color is shifted from blue to yellow.

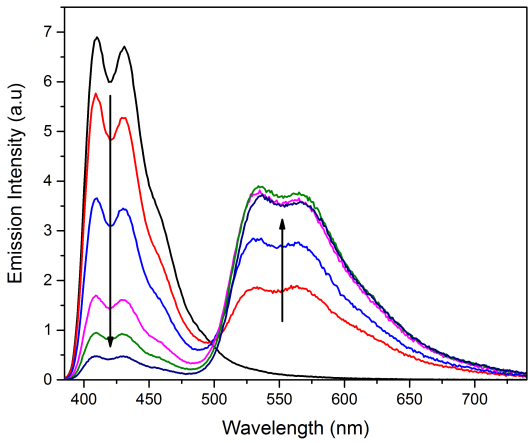

Figure 27. Fluorescence emission spectra (λ_{ex} = 375 nm) of **DAE** and **DPA** in polymer micelles. Step-wise UV-induced (254 nm) isomerization and generation of fluorescent acceptor **DAE$_c$** result in donor emission quenching with concomitant sensitization and emission of the acceptor.

The emission spectra in Figure 27 were converted into CIE coordinates, which represent the perceived color of each distinct spectral signature (see Figure 28). The dichromatic additive mixing of **DPA** and **DAE$_c$** emission colors results in a vector of possible colors in CIE-space.

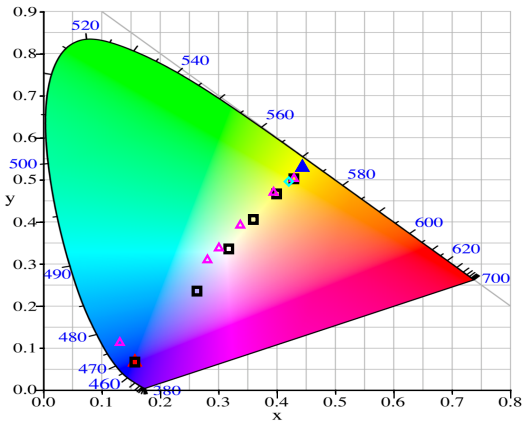

Figure 28. CIE diagram representing the changes in emission-color arising from the interconversion between **DAE$_o$** and **DAE$_c$.** The UV-induced change from pure blue **DPA** emission toward the yellow emission of FRET-acceptor **DAE$_c$** is shown in black hollow square. The purple hollow triangles represent the reversible isomerization back to **DAE$_o$** using 523nm green LED light. The tilted cyano square represent the end-point of a second UV-induced isomerization to **DAE$_c$**.

The initial CIE coordinate (0.16, 0.07) corresponds to pure **DPA** emission (red triangle). Upon UV-induced isomerization of **DAE$_o$** to **DAE$_c$**, the contribution from the sensitized acceptor

emission increases while simultaneously quenching the emission of the donor. Consequently, the perceived color gradually shifts towards that of the yellow **DAE$_c$** emission (hollow black square). It should be noted that, while moving along the resulting CIE trajectory, the system passes through the point (0.32, 0.33). As pure white light is represented by CIE coordinate (0.33, 0.33), the system displays virtually perfect white light generation. Finally, upon complete isomerization into **DAE$_c$**, the system ends up at the CIE coordinate (0.43, 0.51), almost reaching the CIE coordinate (0.44, 0.53) of pure **DAE$_c$** emission (blue triangle). Thus, the displayed change in emission color spans almost the complete range of pure **DPA** and **DAE$_c$** emission, implying that the dynamic range of the color switching is essentially maximized. Further, the CIE diagram in Figure 28 presents the perceived emission color during the reversal to open-form **DAEo** with irradiation with 523nm green LED (purple hollow triangle).

Figure 29 shows the emission spectra of the cocktail of **DPA** (3.5 µM) and **DAE** (2 µM) in both the open and closed form, as well as reference micelles of **DPA** and **DAE** alone (with equivalent concentrations). Comparing the spectrum of pure **DPA** (black line) with the **DPA-DAE$_o$** cocktail (green line), it is observed that the introduction of **DAE$_o$** induces a 43% quenching of the original **DPA** emission.

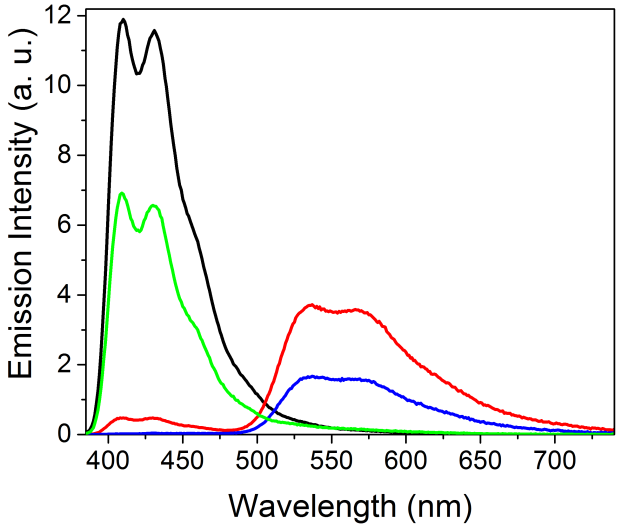

Figure 29. Emission spectra of **DPA** alone (black line), **DAE$_c$** alone (blue line), the cocktail **DPA** + **DAE$_o$** (green line), and **DPA** + **DAE$_c$** (red line), all in water dispersions of the polymer micelles. The concentration of the respective species was the same in all experiments (3.5 μM for **DPA** and 2 μM for **DAE**).

As FRET-based quenching is excluded, a possible explanation could be either the formation of a ground-state complex or quenching *via* photoinduced electron-transfer processes between **DPA** and **DAE$_o$**. TR-SPC measurements are in support of the latter, as they show a decrease of the average **DPA** excited-state lifetime from 7.5 ns to 4.2 ns in the presence of **DAE$_o$**. Thus, the quenching must be dynamic in nature, as the formation of a ground-state complex would have no effect on the excited-state lifetime. Determination of the relevant redox potentials show that electron-transfer reactions between **DPA** and **DAE$_o$** are indeed thermodynamically favorable.

In addition, further support is gained from the fact that the steady-state emission quenching (43%) is in strong agreement with the resulting quenching efficiency (44%) determined by the changes in excited-state lifetime.

Upon complete UV-induced isomerization of **DAE$_o$** to **DAE$_c$** in the **DPA-DAE** cocktail (red line), 96% quenching of the **DPA** emission intensity with a concomitant increase in the **DAE$_c$** emission intensity is observed. The increase in **DAE$_c$** emission is attributed to both an increase in FRET-sensitization as well as a component of directly excited **DAE$_c$**. The contribution in emission intensity associated with the direct excitation of **DAE$_c$** is illustrated by the reference micelle containing only **DAE$_c$** (2μM, blue line). Accounting for the emission intensity arising from direct excitation, the efficiency of the FRET communication was determined to 45%, which is significantly lower than the observed 96% in the steady-state quenching of **DPA**. This discrepancy is again attributed to non-radiative quenching of the excited-state **DPA*** by a thermodynamically favorable PET process, however, this time to **DAE$_c$**. The corresponding TR-SPC measurements are in good agreement with the observed steady-state emission, indicating a 91% quenching efficiency, as the average **DPA** lifetime decreases from 7.5 ns to 0.7 ns upon the introduction of **DAE$_c$**. TR-SPC measurements of the acceptor show no changes in the average **DAE$_c$** excited-state lifetime with and without the presence of **DPA** (both determined to 2.5 ns). Hence, any PET processes proceeding from excited-state **DAE$_c$** can be excluded and are in agreement with the much less favorable driving forces for these processes. Studies of micelles containing only **DPA** or **DAE** (of varying concentrations) show no indication of self-quenching as the increase in steady-state emission intensity was proportional to the increase in concentration. Furthermore, no significant changes in the corresponding TR-SPC lifetimes were observed.

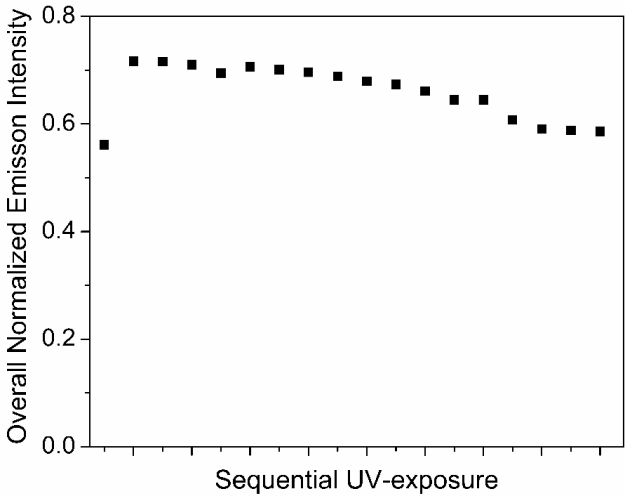

Figure 30. Overall normalized emission intensity as function of UV-exposure the DPA-DAE cocktail.

The combination of multiple excited-state interactions between **DPA**, and the two photochromic forms; **DTE$_o$** and **DTE$_c$**, gives rise to variations in total emission intensity with

sequential UV-irradiation as well as increasing concentration of **DAE$_c$** (Figure 30). Initially, the effective fluorescence quantum yield is 0.57 (due to the 43% PET-based quenching induced by **DAE$_o$**) and is dominated by the blue emission of the fluorophore **DPA**. Upon the first segmental UV-irradiation, the overall emission intensity increases. This is ascribed to the activation of the long-range FRET communication with concomitant decrease of the short-range deactivation of **DPA*** via PET, as well as an increase in directly excited **DAE$_c$**. Subsequent UV-exposure results in a minor decrease in overall emission and is attributed to the increased non-radiative deactivation of **DPA*** *via* PET to **DAE$_c$**, which becomes more competitive with the FRET process as the **DAE$_c$** concentration increases.

In summary, paper IV presents the realization of a FRET-based self-assembled micellar system capable of reversible photochromic regulation of emission color through photonic stimulation. During operation the system traverses the CIE coordinate (0.32, 0.33) and achieves virtually perfect white light.

8. Concluding remarks

The aim of this work has been to investigate photochromic switching as a means to gain photonic control of molecular level phenomena. The resulting studies show an interesting illustration of the versatility of the photochromic compounds and the many ways in which photonic modulation of fluorescence emission can be used to provide various molecular functions and devices.

In paper I and II, we successfully showed that photochromic systems can be used for the implication of all-photonic molecular logic functions. Both these studies qualify as proof-of-principle investigations and do not offer any competitive real-life application as compared to their already existing silicon-based electronic equivalents. In order to fully realize the potential of molecular logic systems, we must arrive at a point where the photoswitching of each photochromic element can be both controlled and read individually. Our presented systems instead operate on an ensemble of molecules in solution, giving an average fluorescence response and switching times of seconds or even minutes for a single operative cycle. Thus, I believe that any possible competitive application in terms of information processing should be realized in the form of a solid state device with arrays of highly organized molecular logic gates. Still, the multidirectional emission of fluorescence poses yet a problem to be solved, as does the inherent loss in photon energy in system involving FRET processes. Thus, the most realistic application of photochromic compounds may lie within two-photon 3D high density memory storage.

In paper III, we demonstrated that the photoswitchable DNA-binding of a photochromic spiropyran to a DNA-scaffold enables the reversible gating of the flow of excitation energy between an appended donor-acceptor pair. As the binding density of the FRET-interrupting MCH^+ species can be controlled by the amount of UV-light provided, the system exhibits an analog “transistor-like” FRET response and the fluorescence emission intensity can be tuned gradually. Although the presented system only exhibits a one-step FRET communication, the operative principle could in theory be extended to reversibly gate the excitation energy flow in multicomponent FRET cascades of photonic DNA wires. Further investigation in this direction could in the future result in photonic DNA structures with multiple excitation energy flow patterns (functionalized DNA origami) where the photochromic molecules act as switching stations, directing the flow of excitation energy between different paths.

In paper IV, we showed that the photoswitching of a photochromic diarylethene in a donor-acceptor (FRET) system in micellar aggregates enables the reversible tuning of the observed emission color. Furthermore, virtually perfect white light fluorescence was achieved with CIE coordinate (0.32, 0.33). Even though the intended function was realized, the system suffers from a reduced donor fluorescence quantum yield due to the photoinduce electron transfer interaction with both the isomeric forms of the photochromic diarylethene. This effect (the PET quenching) was diminished in experiments performed with lower intramicellar dye concentration and, consequently, longer average donor-acceptor distances. Also, the increased donor-acceptor separation reduced the FRET efficiency and thus decreased the ability to fully tune the emission color to that of the yellow diarylethene emission. To achieve the full

switching potential implied by this system, the acceptor and the donor need to be spatially organized in such a way that efficient energy transfer switching is enabled while simultaneously inhibiting the electron transfer reaction. In fact, the project in paper IV started with a covalent linked design of a fluorophore-photochrome dyad. Here, the FRET reactions were completely outcompeted by efficient PET reactions. The following efforts in synthesizing a dyad where the PET reactions were suppressed were unfruitful. Finally, what has been done in the presented dichromatic system for photochromic color tuning could also be done with a trichromatic approach by using two distinct fluorescent photochromic acceptors with a common donor fluorophore. Of course, increasing the number of components and processes involved would render such a design more complex. However, if achieved, it could provide photocontrolled emission color tuning within the entire area spanned by their three CIE coordinates.

9. Acknowledgements

First and foremost, I would like to thank my brilliant supervisor **Joakim Andréasson** for all your support throughout my journey as a PhD student. For always taking the time for a pen-and-paper rundown and answering all my questions with great patience.

Shiming Li –The magician on the 9th floor. Without you and your exquisite skills in organic synthesis, none of this would have been possible.

Jesper JR Nilsson and **Martin Hammarson** – Thank you for teaching me the tools of the trade and welcoming me into the group. We've had some great times, both in the lab and at conferences.

Cassandra Fleming – For helping me in the editing process of this thesis and for all the good laughs.

To the colleagues and friends at Physical Chemistry – Spending five years as a PhD student at this department has been wonderful experience and it is all because of you. There is an open and warm atmosphere at this place and I truly will miss all you amazing people ☺

Joachim Wallenstein – My longtime friend and the closest thing I have to a brother. We walked this journey side by side and now it is time for a new chapter. Whatever will be your next step, stay awesome!

Damir Džebo – Thank you for being a great friend. Thank you for all the great conversations about nothing and everything. Thank you for the time we spent sharing offices and all the great laughs.

Mom and Dad – I love you. Thank you for always being there for me and supporting me all the way throughout my journey here at Chalmers. Now it is done. I did it ☺

Valentina Cantatore – My amazing girlfriend. Thank you for always helping me to see myself in the highest light. For all your support and encouragement.

10. References

1. Irie, M. *Chem. Rev.* **2000**, 100, 1685-1716.
2. Berkovic, G., Krongauz, V., and Weiss, V. *Chem. Rev.* **2000**, 100, 1741-1754.
3. Yokoyama, Y. *Chem. Rev.* **2000**, 100, 1717-1740.
4. Irie, M., Fukaminato, T., Matsuda, K., and Kobatake, S. *Chem. Rev.* **2014**, 114, 12174-12277.
5. Bouas-Laurent, H. and Dürr, H. *Pure Appl. Chem.* **2001**, 73, 639-665.
6. Raymo, F.M. and Tomasulo, M. *Chem. Soc. Rev.* **2005**, 34, 327-336.
7. Cusido, J., Deniz, E., and Raymo, F.M. *Eur. J. Org. Chem.* **2009**, 2009, 2031-2045.
8. Yildiz, I., Impellizzeri, S., Deniz, E., McCaughan, B., et al. *J. Am. Chem. Soc.* **2010**, 133, 871-879.
9. Raymo, F.M. *Isr. J. Chem.* **2013**, 53, 247-255.
10. Andréasson, J. and Pischel, U. *Chem. Soc. Rev.* **2010**, 39, 174-188.
11. Andréasson, J. and Pischel, U. *Isr. J. Chem.* **2013**, 53, 236-246.
12. Andréasson, J. and Pischel, U. *Chem. Soc. Rev.* **2015**, 44, 1053-1069.
13. Straight, S.D., Andréasson, J., Kodis, G., Bandyopadhyay, S., et al. *J. Am. Chem. Soc.* **2005**, 127, 9403-9409.
14. Andréasson, J., Straight, S.D., Kodis, G., Park, C.-D., et al. *J. Am. Chem. Soc.* **2006**, 128, 16259-16265.
15. Andréasson, J., Straight, S.D., Bandyopadhyay, S., Mitchell, R.H., et al. *Angew. Chem. Int. Ed.* **2007**, 46, 958-961.
16. Andréasson, J., Straight, S.D., Bandyopadhyay, S., Mitchell, R.H., et al. *The Journal of Physical Chemistry C* **2007**, 111, 14274-14278.
17. Straight, S.D., Liddell, P.A., Terazono, Y., Moore, T.A., et al. *Adv. Funct. Mater.* **2007**, 17, 777-785.
18. Andréasson, J., Straight, S.D., Moore, T.A., Moore, A.L., et al. *J. Am. Chem. Soc.* **2008**, 130, 11122-11128.
19. Andréasson, J., Straight, S.D., Moore, T.A., Moore, A.L., et al. *Chemistry–A European Journal* **2009**, 15, 3936-3939.
20. Andréasson, J., Pischel, U., Straight, S.D., Moore, T.A., et al. *J. Am. Chem. Soc.* **2011**, 133, 11641-11648.
21. De Silva, A.P. *Nature Materials* **2005**, 4, 15-16.
22. De Silva, A.P. and Uchiyama, S. *Nature Nanotechnology* **2007**, 2, 399-410.
23. Pischel, U. *Angew. Chem. Int. Ed.* **2007**, 46, 4026-4040.
24. Zhao, Z., Xing, Y., Wang, Z., and Lu, P. *Org. Lett.* **2007**, 9, 547-550.
25. Meng, X., Zhu, W., Zhang, Q., Feng, Y., et al. *The Journal of Physical Chemistry B* **2008**, 112, 15636-15645.
26. Silvi, S., Constable, E.C., Housecroft, C.E., Beves, J.E., et al. *Chemistry–A European Journal* **2009**, 15, 178-185.
27. Hammarson, M., Andersson, J., Li, S., Lincoln, P., et al. *Chem. Commun.* **2010**, 46, 7130-7132.
28. Prasanna de Silva, A. *Chemistry–An Asian Journal* **2011**, 6, 750-766.
29. Gust, D., Andréasson, J., Pischel, U., Moore, T.A., et al. *Chem. Commun.* **2012**, 48, 1947-1957.
30. Remón, P., Li, S., Grøtli, M., Pischel, U., et al. *Chem. Commun.* **2016**, 52, 4659-4662.
31. Natali, M. and Giordani, S. *Chem. Soc. Rev.* **2012**, 41, 4010-4029.
32. Shinkai, S. and Manabe, O. (1984) Photocontrol of ion extraction and ion transport by photofunctional crown ethers. In *Host Guest Complex Chemistry III*, pp. 67-104, Springer.
33. Collins, G., Ewing, K., Bowen, C., and Winkler, J. *Chem. Commun.* **1999**, 321-322.
34. Paramonov, S.V., Lokshin, V., and Fedorova, O.A. *Journal of Photochemistry and Photobiology C: Photochemistry Reviews* **2011**, 12, 209-236.
35. Lee, M.H., Kim, J.Y., Han, J.H., Bhuniya, S., et al. *J. Am. Chem. Soc.* **2012**, 134, 12668-12674.
36. Zhu, L., Wu, W., Zhu, M.-Q., Han, J.J., et al. *J. Am. Chem. Soc.* **2007**, 129, 3524-3526.
37. Schierling, B., Noël, A.-J., Wende, W., Volkov, E., et al. *Proceedings of the National Academy of Sciences* **2010**, 107, 1361-1366.

38. Nishioka, H., Liang, X., Kato, T., and Asanuma, H. *Angew. Chem. Int. Ed.* **2012**, 51, 1165-1168.
39. Hayakawa, R., Higashiguchi, K., Matsuda, K., Chikyow, T., et al. *ACS applied materials & interfaces* **2013**, 5, 3625-3630.
40. Broman, S.L., Lara-Avila, S., Thisted, C.L., Bond, A.D., et al. *Adv. Funct. Mater.* **2012**, 22, 4249-4258.
41. Sendler, T., Luka-Guth, K., Wieser, M., Wolf, J., et al. *Advanced Science* **2015**, 2.
42. Chen, K.J., Laurent, A.D., and Jacquemin, D. *The Journal of Physical Chemistry C* **2014**, 118, 4334-4345.
43. Saika, T., Iyoda, T., Honda, K., and Shimidzu, T. *J. Chem. Soc., Chem. Commun.* **1992**, 591-592.
44. Walz, J., Ulrich, K., Port, H., Wolf, H.C., et al. *Chem. Phys. Lett.* **1993**, 213, 321-324.
45. Port, H., Hartschuh, A., Hennrich, M., Wolf, H., et al. *Molecular Crystals and Liquid Crystals* **2000**, 344, 145-150.
46. Endtner, J.M., Effenberger, F., Hartschuh, A., and Port, H. *J. Am. Chem. Soc.* **2000**, 122, 3037-3046.
47. Myles, A.J. and Branda, N.R. *J. Am. Chem. Soc.* **2001**, 123, 177-178.
48. Otsuki, J., Suka, A., Yamazaki, K., Abe, H., et al. *Chem. Commun.* **2004**, 1290-1291.
49. Terazono, Y., Kodis, G., Andréasson, J., Jeong, G., et al. *The Journal of Physical Chemistry B* **2004**, 108, 1812-1814.
50. Yildiz, I., Deniz, E., and Raymo, F.M. *Chem. Soc. Rev.* **2009**, 38, 1859-1867.
51. Deniz, E., Sortino, S., and Raymo, F.i.M. *The Journal of Physical Chemistry Letters* **2010**, 1, 3506-3509.
52. Deniz, E., Tomasulo, M., Cusido, J., Yildiz, I., et al. *The Journal of Physical Chemistry C* **2012**, 116, 6058-6068.
53. Inada, T., Uchida, S., and Yokoyama, Y. *Chem. Lett.* **1997**, 321-322.
54. Bahr, J.L., Kodis, G., de la Garza, L., Lin, S., et al. *J. Am. Chem. Soc.* **2001**, 123, 7124-7133.
55. Norsten, T.B. and Branda, N.R. *J. Am. Chem. Soc.* **2001**, 123, 1784-1785.
56. Ramsteiner, I., Hartschuh, A., and Port, H. *Chem. Phys. Lett.* **2001**, 343, 83-90.
57. Giordano, L., Jovin, T.M., Irie, M., and Jares-Erijman, E.A. *J. Am. Chem. Soc.* **2002**, 124, 7481-7489.
58. Díaz, S.A., Giordano, L., Jovin, T.M., and Jares-Erijman, E.A. *Nano Lett.* **2012**, 12, 3537-3544.
59. Irie, M., Fukaminato, T., Sasaki, T., Tamai, N., et al. *Nature* **2002**, 420, 759-760.
60. Harbron, E.J., Vicente, D.A., and Hoyt, M.T. *The Journal of Physical Chemistry B* **2004**, 108, 18789-18792.
61. Uno, K., Niikura, H., Morimoto, M., Ishibashi, Y., et al. *J. Am. Chem. Soc.* **2011**, 133, 13558-13564.
62. Chibisov, A.K. and Görner, H. *The Journal of Physical Chemistry A* **1997**, 101, 4305-4312.
63. Liang, Y., Dvornikov, A.S., and Rentzepis, P.M. *J. Mater. Chem.* **2000**, 10, 2477-2482.
64. Goerner, H., Fischer, C., Gierisch, S., and Daub, J. *The Journal of Physical Chemistry* **1993**, 97, 4110-4117.
65. Weber, C., Rustemeyer, F., and Dürr, H. *Adv. Mater.* **1998**, 10, 1348-1351.
66. Su, W., Bonnard, V., and Burley, G.A. *Chemistry–A European Journal* **2011**, 17, 7982-7991.
67. Kawahara, S.-i., Uchimaru, T., and Murata, S. *Chem. Commun.* **1999**, 563-564.
68. Ohya, Y., Yabuki, K., Hashimoto, M., Nakajima, A., et al. *Bioconjugate Chem.* **2003**, 14, 1057-1066.
69. Heilemann, M., Tinnefeld, P., Sanchez Mosteiro, G., Garcia Parajo, M., et al. *J. Am. Chem. Soc.* **2004**, 126, 6514-6515.
70. Hannestad, J.K., Sandin, P., and Albinsson, B. *J. Am. Chem. Soc.* **2008**, 130, 15889-15895.
71. Hannestad, J.K., Gerrard, S.R., Brown, T., and Albinsson, B. *Small* **2011**, 7, 3178-3185.
72. Dutta, P.K., Varghese, R., Nangreave, J., Lin, S., et al. *J. Am. Chem. Soc.* **2011**, 133, 11985-11993.
73. Garo, F. and Häner, R. *Angew. Chem.* **2012**, 124, 940-943.
74. Swaminathan, S., Garcia-Amorós, J., Fraix, A., Kandoth, N., et al. *Chem. Soc. Rev.* **2014**, 43, 4167-4178.

75. Swaminathan, S., Fowley, C., McCaughan, B., Cusido, J., et al. *J. Am. Chem. Soc.* **2014**, 136, 7907-7913.
76. Hartley, G. *Nature* **1937**, 140, 281.
77. Fischer, E. and Hirshberg, Y. (1952) Formation of coloured forms of spirans by low-temperature irradiation. pp. 4522-4524, ROYAL SOC CHEMISTRY THOMAS GRAHAM HOUSE, SCIENCE PARK, MILTON RD, CAMBRIDGE CB4 0WF, CAMBS, ENGLAND.
78. Renth, F., Siewertsen, R., and Temps, F. *Int. Rev. Phys. Chem.* **2013**, 32, 1-38.
79. Yokoyama, Y., Tanaka, T., Yamane, T., and Kurita, Y. *Chem. Lett.* **1991**, 1125-1128.
80. Stobbe, H. *Berichte der deutschen chemischen Gesellschaft* **1907**, 40, 3372-3382.
81. Chakraborty, D., Sleigh, T., Stevenson, R., Swoboda, G.A., et al. *The Journal of Organic Chemistry* **1966**, 31, 3342-3345.
82. Hart, R., Heller, H., and Salisbury, K. *Chemical Communications (London)* **1968**, 1627-1628.
83. Yokoyama, Y., Yamane, T., and Kurita, Y. *J. Chem. Soc., Chem. Commun.* **1991**, 1722-1724.
84. Tomoda, A., Tsuboi, H., Kaneko, A., and Matsushima, R. *Nippon Kagaku Kaishi* **1992**, 1071-1071.
85. Matsui, F., Taniguchi, H., Yokoyama, Y., Sugiyama, K., et al. *Chem. Lett.* **1994**, 1869-1872.
86. Liang, Y., Dvornikov, A.S., and Rentzepis, P.M. *Optics Communications* **2003**, 223, 61-66.
87. Liang, Y., Dvornikov, A., and Rentzepis, P. *Res. Chem. Intermed.* **1998**, 24, 905-914.
88. Tian, H. and Yang, S. *Chem. Soc. Rev.* **2004**, 33, 85-97.
89. Yun, C., You, J., Kim, J., Huh, J., et al. *Journal of Photochemistry and Photobiology C: Photochemistry Reviews* **2009**, 10, 111-129.
90. Irie, M. and Mohri, M. *The Journal of Organic Chemistry* **1988**, 53, 803-808.
91. Nakamura, S. and Irie, M. *The Journal of Organic Chemistry* **1988**, 53, 6136-6138.
92. Hanazawa, M., Sumiya, R., Horikawa, Y., and Irie, M. *J. Chem. Soc., Chem. Commun.* **1992**, 206-207.
93. Matsuda, K. and Irie, M. *Journal of Photochemistry and Photobiology C: Photochemistry Reviews* **2004**, 5, 169-182.
94. Nilsson, J.R., O'Sullivan, M.C., Li, S., Anderson, H.L., et al. *Chem. Commun.* **2015**, 51, 847-850.
95. Woodward, R.B. and Hoffmann, R. *Angewandte Chemie International Edition in English* **1969**, 8, 781-853.
96. Fukaminato, T., Doi, T., Tamaoki, N., Okuno, K., et al. *J. Am. Chem. Soc.* **2011**, 133, 4984-4990.
97. Pärs, M., Hofmann, C.C., Willinger, K., Bauer, P., et al. *Angew. Chem. Int. Ed.* **2011**, 50, 11405-11408.
98. Kärnbratt, J., Hammarson, M., Li, S., Anderson, H.L., et al. *Angew. Chem.* **2010**, 122, 1898-1901.
99. Lee, P.H.-M., Ko, C.-C., Zhu, N., and Yam, V.W.-W. *J. Am. Chem. Soc.* **2007**, 129, 6058-6059.
100. Zhang, J., Tan, W., Meng, X., and Tian, H. *J. Mater. Chem.* **2009**, 19, 5726-5729.
101. Zou, Q., Jin, J., Xu, B., Ding, L., et al. *Tetrahedron* **2011**, 67, 915-921.
102. Zou, Q., Li, X., Zhang, J., Zhou, J., et al. *Chem. Commun.* **2012**, 48, 2095-2097.
103. Corredor, C.C., Huang, Z.L., and Belfield, K.D. *Adv. Mater.* **2006**, 18, 2910-2914.
104. Zhu, W., Yang, Y., Métivier, R., Zhang, Q., et al. *Angew. Chem. Int. Ed.* **2011**, 50, 10986-10990.
105. Soh, N., Yoshida, K., Nakajima, H., Nakano, K., et al. *Chem. Commun.* **2007**, 5206-5208.
106. Zou, Y., Yi, T., Xiao, S., Li, F., et al. *J. Am. Chem. Soc.* **2008**, 130, 15750-15751.
107. Minkin, V.I. *Chem. Rev.* **2004**, 104, 2751-2776.
108. Hammarson, M., Nilsson, J.R., Li, S., Beke-Somfai, T., et al. *The Journal of Physical Chemistry B* **2013**, 117, 13561-13571.
109. Görner, H. *PCCP* **2001**, 3, 416-423.
110. Klajn, R. *Chem. Soc. Rev.* **2014**, 43, 148-184.
111. Hammarson, M., Nilsson, J.R., Li, S., Lincoln, P., et al. *Chemistry–A European Journal* **2014**, 20, 15855-15862.
112. Lukyanov, B. and Lukyanova, M. *Chemistry of Heterocyclic Compounds* **2005**, 41, 281-311.
113. Zhang, J., Zou, Q., and Tian, H. *Adv. Mater.* **2013**, 25, 378-399.

114. Lutsyk, P., Janus, K., Sworakowski, J., Generali, G., et al. *The Journal of Physical Chemistry C* **2011**, 115, 3106-3114.
115. Nilsson, J.R., Li, S., Önfelt, B., and Andréasson, J. *Chem. Commun.* **2011**, 47, 11020-11022.
116. Qi, Q., Qian, J., Ma, S., Xu, B., et al. *Chemistry–A European Journal* **2015**, 21, 1149-1155.
117. Guo, X., Zhang, D., Zhou, Y., and Zhu, D. *The Journal of organic chemistry* **2003**, 68, 5681-5687.
118. Chernyshev, A.V., Metelitsa, A.V., Gaeva, E.B., Voloshin, N.A., et al. *J. Phys. Org. Chem.* **2007**, 20, 908-916.
119. Delaire, J.A. and Nakatani, K. *Chem. Rev.* **2000**, 100, 1817-1846.
120. Fernández-Acebes, A. and Lehn, J.M. *Chemistry–A European Journal* **1999**, 5, 3285-3292.
121. Jin, M., Lu, R., Bao, C.Y., Xu, T.H., et al. *Opt. Mater.* **2004**, 26, 85-88.
122. Bossi, M., Belov, V., Polyakova, S., and Hell, S.W. *Angew. Chem. Int. Ed.* **2006**, 45, 7462-7465.
123. Petriella, M., Deniz, E., Swaminathan, S., Roberti, M.J., et al. *Photochem. Photobiol.* **2013**, 89, 1391-1398.
124. Cheng, H.-B., Zhang, H.-Y., and Liu, Y. *J. Am. Chem. Soc.* **2013**, 135, 10190-10193.
125. Andréasson, J., Kodis, G., Terazono, Y., Liddell, P.A., et al. *J. Am. Chem. Soc.* **2004**, 126, 15926-15927.
126. Tsuchiya, S. *J. Am. Chem. Soc.* **1999**, 121, 48-53.
127. Archut, A., Azzellini, G.C., Balzani, V., De Cola, L., et al. *J. Am. Chem. Soc.* **1998**, 120, 12187-12191.
128. Rodríguez-Redondo, J.L., Sastre-Santos, Á., Fernández-Lázaro, F., Soares, D., et al. *Chem. Commun.* **2006**, 1265-1267.
129. Kawai, T., Sasaki, T., and Irie, M. *Chem. Commun.* **2001**, 711-712.
130. Osuka, A., Fujikane, D., Shinmori, H., Kobatake, S., et al. *The Journal of organic chemistry* **2001**, 66, 3913-3923.
131. Jukes, R.T., Adamo, V., Hartl, F., Belser, P., et al. *Inorg. Chem.* **2004**, 43, 2779-2792.
132. Wang, S., Shen, W., Feng, Y., and Tian, H. *Chem. Commun.* **2006**, 1497-1499.
133. Liddell, P.A., Kodis, G., Moore, A.L., Moore, T.A., et al. *J. Am. Chem. Soc.* **2002**, 124, 7668-7669.
134. CIE, C. (1932) Commission Internationale de l'Eclairage Proceedings, 1931. Cambridge University Press Cambridge.
135. Li, C. and Liu, S. *Chem. Commun.* **2012**, 48, 3262-3278.
136. Mukherjee, S. and Thilagar, P. *Dyes and Pigments* **2014**, 110, 2-27.
137. Wu, H., Ying, L., Yang, W., and Cao, Y. *Chem. Soc. Rev.* **2009**, 38, 3391-3400.
138. Chen, J., Zhang, P., Fang, G., Yi, P., et al. *The Journal of Physical Chemistry B* **2012**, 116, 4354-4362.
139. Kim, S., Yoon, S.-J., and Park, S.Y. *J. Am. Chem. Soc.* **2012**, 134, 12091-12097.
140. Zhu, L., Li, X., Zhang, Q., Ma, X., et al. *J. Am. Chem. Soc.* **2013**, 135, 5175-5182.
141. Coppo, P., Duati, M., Kozhevnikov, V.N., Hofstraat, J.W., et al. *Angew. Chem.* **2005**, 117, 1840-1844.
142. Praveen, V.K., Ranjith, C., and Armaroli, N. *Angew. Chem. Int. Ed.* **2014**, 53, 365-368.
143. Feng, H.-T., Xiong, J.-B., Zheng, Y.-S., Pan, B., et al. *Chem. Mater.* **2015**, 27, 7812-7819.
144. Jiang, B.-P., Guo, D.-S., Liu, Y.-C., Wang, K.-P., et al. *ACS nano* **2014**, 8, 1609-1618.
145. Kim, H.J., Whang, D.R., Gierschner, J., Lee, C.H., et al. *Angew. Chem. Int. Ed.* **2015**, 54, 4330-4333.
146. Huynh, H.V., He, X., and Baumgartner, T. *Chem. Commun.* **2013**, 49, 4899-4901.
147. Liu, D., Zhang, Z., Zhang, H., and Wang, Y. *Chem. Commun.* **2013**, 49, 10001-10003.
148. Täuscher, E., Weiß, D., Beckert, R., Fabian, J., et al. *Tetrahedron Lett.* **2011**, 52, 2292-2294.
149. Yang, Y., Lowry, M., Schowalter, C.M., Fakayode, S.O., et al. *J. Am. Chem. Soc.* **2006**, 128, 14081-14092.
150. Karpiuk, J., Karolak, E., and Nowacki, J. *PCCP* **2010**, 12, 8804-8809.
151. Maity, A., Ali, F., Agarwalla, H., Anothumakkool, B., et al. *Chem. Commun.* **2015**, 51, 2130-2133.

152. Park, S., Kwon, J.E., Kim, S.H., Seo, J., et al. *J. Am. Chem. Soc.* **2009**, 131, 14043-14049.
153. de Silva, P.A., Gunaratne, N.H., and McCoy, C.P. *Nature* **1993**, 364, 42-44.
154. Credi, A. *Angew. Chem. Int. Ed.* **2007**, 46, 5472-5475.
155. Szaciłowski, K. *Chem. Rev.* **2008**, 108, 3481-3548.
156. Nakagawa, T., Hasegawa, Y., and Kawai, T. *Chem. Commun.* **2009**, 5630-5632.
157. Wang, J.C. *Proceedings of the National Academy of Sciences* **1979**, 76, 200-203.
158. Richards, A.D. and Rodger, A. *Chem. Soc. Rev.* **2007**, 36, 471-483.
159. Lerman, L. *J. Mol. Biol.* **1961**, 3, 18IN13-30IN14.
160. Teo, Y.N. and Kool, E.T. *Chem. Rev.* **2012**, 112, 4221-4245.
161. Lodge, T.P. *Macromol. Chem. Phys.* **2003**, 204, 265-273.
162. Webber, S. *The Journal of Physical Chemistry B* **1998**, 102, 2618-2626.
163. Riess, G. *Prog. Polym. Sci.* **2003**, 28, 1107-1170.
164. Okhapkin, I.M., Makhaeva, E.E., and Khokhlov, A.R. (2006) Water solutions of amphiphilic polymers: nanostructure formation and possibilities for catalysis. In *Conformation-Dependent Design of Sequences in Copolymers I*, pp. 177-210, Springer.
165. Kale, T.S., Klaikherd, A., Popere, B., and Thayumanavan, S. *Langmuir* **2009**, 25, 9660-9670.
166. Owen, S.C., Chan, D.P., and Shoichet, M.S. *Nano Today* **2012**, 7, 53-65.
167. Chen, J., Zhang, P., Fang, G., Yi, P., et al. *The Journal of Physical Chemistry B* **2011**, 115, 3354-3362.
168. Harbron, E.J., Davis, C.M., Campbell, J.K., Allred, R.M., et al. *The Journal of Physical Chemistry C* **2009**, 113, 13707-13714.
169. Davis, C.M., Childress, E.S., and Harbron, E.J. *The Journal of Physical Chemistry C* **2011**, 115, 19065-19073.
170. Chen, J., Zeng, F., Wu, S., Chen, Q., et al. *Chemistry–A European Journal* **2008**, 14, 4851-4860.
171. Chen, J., Zeng, F., and Wu, S. *ChemPhysChem* **2010**, 11, 1036-1043.
172. Irie, M. and Sayo, K. *The Journal of Physical Chemistry* **1992**, 96, 7671-7674.
173. Ishibashi, Y., Umesato, T., Fujiwara, M., Une, K., et al. *The Journal of Physical Chemistry C* **2015**.